FINAL REPORT

Determination of Optical Water Quality Requirements for Growth of Seagrasses in the Indian River near Ft. pierce, FL, with Emphasis on the Impact of Colored Water Discharges

for

Contract No. C–3311
Between South Florida Water Management District,
West Palm Beach, Florida

and

Smithsonian Institution
Office of Sponsored Projects
Washington, D.C.

by

Charles L. Gallegos
Smithsonian Enviornmental Research Center
P. O. Box 28
Edgewater, MD 21037

September, 1993

I. INTRODUCTION

A. Objective. The Indian River Lagoon Surface Water Improvement and Management (SWIM) Plan establishes the desirability of maintaining and expanding the coverage of lagoon bottom by seagrasses. Increased coverage by seagrasses is expected to directly contribute to improved value of recreational and commercial fisheries because this habitat functions as a contribution to primary productivity, as a refuge for larval and juvenile fish, and as a trap for suspended sediments and stabilizer of bottom sediments. Recent studies (Kenworthy and Haunert 1991; Dennison et al. 1993) have established that seagrass require a long term average of approximately 20% of surface sunlight for survival. This requirement places severe restrictions on the depth distribution of seagrasses. In the Indian River Lagoon where the bottom slopes gently, even slight reductions in the 20% penetration depth can render extensive regions unsuitable for seagrass survival.

This knowledge underscores the need for maintenance of acceptable water quality within the Lagoon, but does not provide adequate guidance as to the acceptable or desirable concentrations of materials that cause light attenuation. Light attenuation cannot be regulated directly; it is a complex function of the materials in the water that selectively absorb and scatter light on a wavelength-specific basis. The objective of this work is to develop and calibrate a model of the diffuse attenuation coefficient (*see below*) for downwelling photosynthetically active radiation (PAR) in the region near Ft. Pierce, FL, and to use the model in conjunction with *in situ* seagrass mapping to assess the impact of colored water discharge from structure C-25 at Taylor Creek on the depth distribution of a nearby seagrass bed.

B. Background. Kenworthy (1992) proposed a five step process for improving the existing transparency standard consisting of: (1) establishment of the existing maximum depth distribution of seagrasses within targeted water bodies; (2) implementation of a systematic water quality sampling program including diffuse attenuation coefficient and functionally related water quality parameters; (3) establishment of seagrass areal coverage goals and the diffuse attenuation necessary to provide the desired coverage given the regional bathymetry; (4) determining the functional relationship between diffuse attenuation and the governing water quality parameters; and (5) implementing a plan to manage the reduction of inputs from the sources considered detrimental to transparency of the water body. This work addresses step 4 of the above plan.

Part I of this report presents the modeling approach, the field and laboratory data, and the results of model calibration and application to water high in dissolved color. Part II presents results of field transects to determine the impact of colored water discharges on the depth

distribution of seagrasses in a bed near Taylor Creek compared with distributions at a site removed from influences of colored discharges.

C. Rationale and Model Development. The empirical descriptor of the light available at a depth in terms of that available at the surface is the diffuse attenuation coefficient of downward propagating irradiance, K_d, defined as

$$K_d = -\frac{1}{z}\ln\left(\frac{E_z}{E_{0^-}}\right) \tag{1}$$

where E_z is the irradiance available at depth z, E_{0^-} is the irradiance just below the surface (0^-) (Morel and Smith 1978). The definition is useful because the decrease in irradiance with depth is approximately exponential. The depth to which, 20% of surface-incident irradiance penetrates, Z_{20}, is easily determined from (1) as

$$Z_{20} = \frac{-\ln(0.20)}{K_d} = \frac{1.61}{K_d} \tag{2}$$

where the negative sign converts depth to positive distance below the water surface.

The diffuse attenuation coefficient is referred to as an apparent optical property (Preisendorfer 1976) because its value depends on the ambient underwater light field. It's magnitude changes as the angular distribution of the underwater light field changes with depth or with cloud cover, and it depends on the sun as a light source. Because of the dependence on the ambient light field, K_d cannot, in principle, be decomposed into contributions due to separate components, although it is sometimes attempted as an approximation (Smith 1982).

Properties that do not depend on the ambient light field either for their definition or for their measurement are called inherent optical properties (Preisendorfer 1976; Kirk 1981). Inherent optical properties, in particular the total absorption coefficient, a_t, and the scattering coefficient, b, have the property that the contributions due to different materials are additive, and the partial contribution due to each material is linear with its concentration. The proportionality constant between, for example, absorption coefficient and the concentration of a constituent is called the optical cross section of the material.

The relationship between K_d and inherent optical properties is the subject of continuing research (Kirk 1991; Gordon 1991), principally by Monte Carlo simulation of the equations of radiative transfer. A useful relationship is one determined by Kirk (1984)

$$K_d = \frac{1}{\mu_0}[a_t^2 + G(\mu_0)a_t b]^{\frac{1}{2}} \quad (3)$$

where μ_0=cosine of the zenith angle of the direct solar beam refracted at the air-water interface (a function of latitude, date, and time of day), and $G(\mu_0)$ is a function of the form

$$G(\mu_0) = g_1\mu_0 - g_2 \quad (4)$$

that modifies the interaction between scattering and absorption; g_1 and g_2 are coefficients that depend on the scattering phase function (an inherent optical property) of the water column and on the optical depth of interest (Kirk 1991). Values of g_1 and g_2 have been determined for depth intervals from the surface down to the 1% penetration depth and for a small depth increment about the 10% penetration depth, both for waters having volume scattering functions typical of turbid coastal water (Kirk 1984). Unfortunately, g_1 and g_2 have not been determined for the depth interval from the surface down to Z_{20}, the approximate depth at which seagrasses can survive. In the ensuing analysis, the coefficients determined for the surface down to the 1% penetration depth were used.

To predict K_d from water quality measurements it is necessary to specify a_t and b in terms of optically important water quality concentrations. As indicated above, a_t may be expressed as the sum

$$a_t = a_y + a_d + a_{ph} + a_w \quad (5)$$

where the subscripts indicate contributions due to dissolved yellow substance (y), detrital particulates (d), phytoplankton (ph), and water itself (w). Scattering due to particles far exceeds that due to water itself in estuaries, so that b need not be decomposed into components.

In general, both a_t and b may depend on wavelength, λ. Although some studies have found b to be independent of wavelength (Phillips and Kirk 1984; Witte et al. 1982), $1/\lambda$ dependence has been suggested (Morel and Gentili 1991), which was used here, with $b(550)$=[Turb] (see e.g. Vant 1990; Weidemann and Bannister 1986). Thus scattering was represented by the equation

$$b(\lambda) = \left(\frac{550}{\lambda}\right)[\text{Turb}] \quad (6).$$

The wavelength dependence of a_y in the visible region of the spectrum may be expressed

simply as a negative exponential (Bricaud et al. 1981)

$$a_y(\lambda) = g_{440}\exp[-s_y(\lambda-440)] \quad (7)$$

where g_{440}=absorption by dissolved yellow matter (gelbstoff) at 440 nm, and s_y=spectral slope; g_{440} was recently proposed as a measure of water color (Cuthbert and Del Giorgio 1992) and correlates well with color as conventionally measured in Pt. units (Bowling et al. 1986).

Typically measurements of a_d, absorption by (mineral and organic) particulate detritus, decrease exponentially in the visible domain to some asymptote in the longwave (λ>700 nm) region of the spectrum (see below, Figure 1). Previous authors (Roessler et al. 1989; Gallegos et al. 1990) have subtracted the longwave asymptote and used expressions similar to equation (7) to model a_d. This procedure attributes all in situ absorption at λ>700 nm to water alone. Previously, Gallegos et al. (1990) estimated b from measurements of $K_d(720)$ by rearranging equation 3 and assuming $a_t(720) \approx a_w(720)$. More recently (Gallegos in press) it was found that attributing all absorption in the 720 nm waveband to water alone produced estimated scattering coefficients that seemed too high. In one case b estimated by the old procedure was >100 m^{-1}, and estimates were always well in excess of measured turbidity. The variable longwave asymptote in the measurements of a_d correlated well with both suspended solids and with turbidity (see below, Results). When longwave absorption by particulate detritus was added to $a_w(720)$ the resulting estimates of b were compatible with equation (6) (*see also* Maske and Haardt, 1987). Thus absorption by nonalgal particulate matter is modeled as

$$a_d(\lambda) = \sigma_d(\lambda)[\text{Turb}] \quad (8a)$$

and

$$\sigma_d(\lambda) = \sigma_{bl} + \sigma_{400}\exp[-s_d(\lambda-400)] \quad (8b)$$

where [Turb]=turbidity (NTU), σ_d is the absorption cross section of turbidity, σ_{bl} is the longwave absorption cross section, σ_{400} scales the absorption maximum at 400 nm, and s_d determines the rate of exponential decrease to σ_{bl}. [Turb] is used in preference to [TSS] because of its superior analytical precision; all regressions had higher coefficients of determination using [Turb] as the independent variable, compared with [TSS].

The wavelength dependencees of a_{ph} and a_w do not have a convenient functional forms. a_{ph} must be expressed in terms of the chlorophyll concentration, [Chl], and tabulated values of chlorophyll-specific absorption, $a^*_{ph}(\lambda)$ (Prieur and Sathyendranath, 1981),

$$a_{ph}(\lambda) = a^*_{ph}[\mathrm{Chl}] \qquad (9).$$

Absorption by water is taken from published values (Smith and Baker 1981).

Equations 6-9 substituted into (5) and (3) express the dependence of spectral diffuse attenuation coefficient on water quality variables. To calculate the penetration of PAR either from the model or from measurements of $K_d(\lambda)$, the spectrum of incident sunlight, E_0^-, (Weast 1980), converted to units of quantum flux density is propagated in 5-nm wavebands to a reference depth, z_r, according to

$$E_{z_r}(\lambda) = E_0(\lambda)\exp[-K_d(\lambda)z_r] \qquad (10).$$

At z_r, $\hat{PAR}_z$ is calculated by numerical integration of $E_{z_r}(\lambda)$ from λ=400 to 700 nm, where the carat distinguishes spectral estimates from field measurements made with broadband sensors. The spectrally estimated diffuse attenuation for PAR, $K_d(\hat{PAR})$ is calculated as

$$K_d(\hat{PAR}) = \frac{1}{z_r}\ln\left(\frac{\hat{PAR}_z}{PAR_0}\right) \qquad (11).$$

Z_{20} for PAR is calculated from $K_d(\hat{PAR})$ by equation (2). Habitat requirements are estimated by varying water quality concentrations, g_{440}, [Turb], and [Chl] over suitable ranges, and determining combinations of variables producing predictions of $Z_{20} \geq$ various target depths.

II. METHODS

A. Field Methods. Profiles of downwelling, cosine-corrected, spectral irradiance were measured using the submersible radiometer described by Gallegos et al. (1990). Wavebands of the spectrum are isolated using interference filters (Corion Corp.) that vary in bandwidths; narrowest bandwidths are used in the region of the spectrum in which diffuse attenuation coefficients change most rapidly. Details of spectral response of the instrument are given by Gallegos et al. (1990). Profiles of downwelling PAR were measured with a Licor 192B underwater quantum sensor.

Voltages for each channel of the spectral radiometer were normalized to readings from a deck cell; percentage of surface irradiance reaching each depth was calculated by dividing the normalized readings by the normalized reading at the surface taken at the start of a profile. Diffuse attenuation coefficients were calculated from the slope of a regression of log-transformed percentages against depth (Gallegos et al. 1990). Diffuse attenuation for PAR was calculated by similar regression of

log-transformed values.

Vertical salinity profiles were measured with a Beckman RS 5–3 induction salinometer. Vertically integrated water samples were collected with a 2-liter Labline Teflon water sampler by slowly lowering and raising the bottle at a constant rate in less time than required to completely fill the bottle. A preliminary cast was made to rinse the sampler and sample bottles. Duplicate casts were made at one station per day for quality control reporting. Samples were placed on ice in a cooler and returned to the laboratory for analysis.

B. Laboratory Methods. Water samples were analyzed for total and mineral suspended solids, chlorophyll *a*, turbidity, color, and absorption by dissolved and particulate matter. All analyses were conducted by standard methods with modifications described in the Research Quality Assurance Plan (RQAP) submitted to and approved by Florida Department of Environmental Regulation, Quality Assurance Section.

For total suspended solids (TSS) a known volume of water (depending on particulate content of the water) was filtered through a tared, precombusted (500 °C, ca. 1 h) GF/F filter. Filters were stored in a desiccator until re-weighed on the same balance as tared. Concentration of TSS was calculated from the weight gain of the filter and volume filtered. Filters were then combusted again at 500 °C for >1 h to burn off organic matter, and re-weighed. Mineral suspended solids (MSS) were determined by difference.

For chlorophyll *a*, a known volume of water was filtered through a Whatman GF/F glass fiber filter, which was frozen for transport to Edgewater, MD. Filters were thawed, placed in a 12-ml centrifuge tube, and extracted overnight at 4 °C in 95 percent acetone. Extracts were centrifuged at 4000 rpm in a clinical centrifuge, and absorbances were read at selected wavelengths; chlorophyll concentrations were calculated by the equations of Jeffrey and Humphrey (1977).

Turbidity was measured with a Hach model 2100A turbidimeter calibrated against formazin standards (Cole Parmer). Dissolved color was measured on water filtered through a Whatman GF/F glass fiber filter by visual comparison in Nessler tubes with standards purchased from Sigma Chemical Co. and mixed as specified in Standard Methods. Color measurements were accompanied by measurements of pH using a VWR pH meter standardized with fresh buffers (also supplied by VWR). g_{440} was measured on water further filtered through a 0.2 µm Nuclepore filter; absorbance was read on a Cary Model 17 spectrophotometer in 10 cm cells against distilled water (filtered 3× through a 0.2 µm Nuclepore filter) blank. Absorbance readings were multiplied by 2.303 to convert to base *e* and divided by 0.1 (dm m^{-1}).

Absorption by particulate matter was measured on material collected on 25 mm GF/F filters. Moistened filters were placed in the entrance port of a Licor 1800–12 integrating sphere and illuminated with a fiber optic light source. Spectral energy flux at the edge of the integrating sphere was measured in 2-nm intervals by an E.G.&G. Gamma spectrometer. Transmission of the particulate material was calculated by normalizing to readings of a moistened, blank filter. Absorption was calculated as ln(1/Transmittance); measurements were converted to units of m^{-1} by multiplying by the area of the filter and dividing by the volume filtered.

pH was read on the sampling vessel within 15 min of sample collection. Turbidity and color were read the same day as collection. Filtrations for chlorophyll *a*, g_{440}, TSS, and MSS were done the same day as sample collection. Analyses on samples transported to Edgewater, MD, were done within times specified in the RQAP.

III. RESULTS

A. Site Selection. Two seagrass beds were chosen for study in relation to optical properties of overlying water quality. One is located at the mouth of Taylor Creek and recieves discharge from the canal structure C-25; the other is located near channel marker 198 of the Intracoastal Waterway. The grassbed stations are designated by the nearest ICW channel marker numbers: 184 is the bed on the west shore of the Indian River just north of the mouth of Taylor Creek; 198 is the unimpacted bed to the south. Further descriptions of the characteristics of each site are given in Part II of this report. In addition, a station was routinely occupied at the furthest upstream location in Taylor Creek that could be reached. This station was occupied to optically characterize the water entering the Lagoon through the canal structure. It is designated Station C-25. Other stations occupied only for irradiance profiles were selected on an *ad hoc* basis to increase the range of water quality conditions encountered. These were Marker 172 near the entrance to Harbor Branch Oceanographic Institute, near Marker 186 near Ft. Pierce Inlet in the turning basin, and near an inlet range marker at coordinates 27° 28.06' N, 80° 18.98' W.

B. Spectral and PAR Diffuse Attenuation Coefficients. A total of 45 profiles of downwelling spectral diffuse attenuation were measured on 3 separate trips to the Fort Pierce area. The data were reported as tables in the progress reports, and, for completeness, are repeated here as originally reported. The number of table entries exceeds the number of stations because at stations within the color plume of Taylor Creek, (C-25 and sometimes 184) diffuse attenuation coefficients were calculated separately for the surface to 0.5 m (designated C-25S and 184S), and for the surface to bottom (designated C-25I and 184I).

Spectra of diffuse attenuation coefficients were typical of coastal waters, having minima in the green region of the visible spectrum, increasing in the blue region due to absorption by color and suspended particulate matter, and in the red region of the spectrum due to absorption by water itself. Spectra of diffuse attenuation coefficient for the least turbid and most turbid profiles from unimpacted stations are shown in Figure 1a. Turbidity, caused by suspended particulate matter, was the primary regulating factor of diffuse attenuation spectra at unimpacted locations.

The effect of high levels of dissolved color was to greatly increase the attenuation in the blue region of the spectrum. Diffuse attenuation coefficients in the 410 nm waveband of the spectral radiometer were as high as 12 m^{-1} at station C-25 in March, when discharge was highest. In December, when dishcarge from Taylor Creek was moderate, the effect of the color occurring as a thin lense could be seen in the difference between diffuse attenuation spectra calculated on the upper 0.5 m *versus* that calculated on the entire profile (Figure 1b). Attenuation was much higher in the blue region at the surface, but the spectra merged in the green and red (wavelength, λ>550 nm) region of the spectrum. In March, when color was highest, removal of energy in the blue was so complete that there was no difference between surface and integrated profiles because there was no blue energy remaining below 0.5 m on which to base attenuation calculations.

C. Water Quality. A wide range of water quality conditions was encountered over the sampling period. Turbidity ranged from 1.4 NTU at Marker 198 in December to 6.25 NTU at the same station in May. Color ranged from 3 Pt. units at a station near Ft. Pierce Inlet in May to 94 Pt. units in the surface water of C-25 in March. At the 2 lagoon stations, chlorophyll *a* was much less variable than color or turbidity, ranging from 1.1 $\mu g\ L^{-1}$ at Marker 198 in March to 7.5 $\mu g\ L^{-1}$ at the same station in May. Although that constitutes a seven-fold range, it is not high enough to substantially affect attenuation given the high background concentrations of suspended particulate matter. Higher concentrations of chlorophyll *a*, up to 30 $\mu g\ L^{-1}$, were measured in Taylor Creek discharge in May. This chlorophyll was of freshwater, not lagoonal origin, and such concentrations were not observed in the lagoon outside of the color plume. Lowest concentrations of total suspended solids (TSS) were ca. 4 $mg\ L^{-1}$, and were found in the surface water at C-25 in March when discharge was high. Highest concentrations of TSS were ca. 40 $mg\ L^{-1}$, and were found near the inlet (Marker 186) in March, and at Marker 198 in May.

Interim water quality samples were collected on 20 January, 28 February, and 30 April 1993. Ranges of parameters that could be measured on frozen samples were within ranges measured when on site. Turbidity varied from 2.1-4.5 NTU, chlorophyll *a* from 1.8-6.8 $\mu g\ L^{-1}$, and TSS from 10-20.2 $mg\ L^{-1}$.

Insight into the factors governing diffuse attenuation in the Lagoon can be gained by examining the interrelationships amongst the various water quality variables. Turbidity, one of the major contributors to attenuation in the Lagoon, is strongly governed by suspended solids (Figure 2a). Two outliers in the relationship occurred at high concentrations of TSS, one at Marker 186 (near Ft. Pierce Inlet) and another at Marker 198 during strong SE winds in May. Strong tidal or wind-driven currents are capable of suspending large, highly aggregated or high specific gravity particles that have less impact on turbidity and attenuation for a given weight. Excluding the 2 outliers, Turbidity is related to TSS by the regression

$$[\text{Turb}] = 0.021*[\text{TSS}] + 0.69 \ (r^2=0.82, n=68) \qquad (12).$$

Total suspended solids consist of suspended mineral particles, adsorbed organic matter, living and dead remains of planktonic organisms, and detritus from decaying macroalgae and higher plants (e.g. marsh grasses, seagrasses, and mangroves). Upon combustion at high temperature, the organic matter volatilizes leaving the mineral fraction behind. In the Indian River Lagoon, total and mineral suspended solids (MSS) were very highly correlated (Figure 2b). The small positive intercept and nearly constant relationship between TSS and MSS indicates that there is a small background organic matter concentration and that the mineral component is a nearly constant fraction of the total. Such a relationship indicates that the organic fraction of the sediment is either adsorbed to the mineral fraction, or that the mineral and organic fractions have a common origin, e.g. *via* resuspension. TSS and MSS were related by the regression equation

$$\text{TSS} = 1.2*[\text{MSS}] + 1.4 \ (r^2 = 0.988, n=64) \qquad (13).$$

The volatile suspended solids, VSS (=TSS - MSS), were poorly correlated (r^2=0.31) with chlorophyll (Chl) everywhere except at C-25 (r^2=0.71, Figure 2c). Assuming volatile suspended solids are ca. 50 percent carbon, the slope of the relationship [6 μg Chl (mg VSS)$^{-1}$] at C-25 would imply a C:Chl ratio of 83 mg C (mg Chl)$^{-1}$, which is not too high to be attributable to phytoplankton. At all other locations, the order-of-magnitude lower slope implies that only a minor fraction of the VSS is actual phytoplankton. The weak correlation suggests that some of the chlorophyll may originate in the same manner as the total suspended solids, probably resuspension of benthic diatoms.

g_{440}, from which $a_y(\lambda)$ is calculated, is not a standard parameter in water quality monitoring programs, although it has been proposed as an alternative measure of color (Cuthbert and Del Giorgio 1992). g_{440} is strongly correlated with color as conventionally measured by the visual comparison method using Nessler tubes and standard Pt. solutions (Figure 2d). Regression

(without intercept) of g_{440} against Color gave

$$g_{440} = 0.074*[\text{Color}] \ (r^2=0.98, n=64) \qquad (14).$$

This relationship is used in the optical model to express $a_y(\lambda)$ in terms of Color.

IV. DELIVERABLES

A. Model Calibration. The main parameters in the model that need to be calibrated on a site-specific basis are σ_{bl}, σ_{400}, and s_d in equation 8b, i.e. the coefficients that determine the specific absorption due to suspended particulate matter. For determination of these coefficients, the stations that were not within the color plume of Taylor Creek were segregated out for analysis. In this way, model calibration and evaluation in relation to the impact of colored water discharge could proceed independently.

In this work, similar to Gallegos (in press), I found that $a_d\lambda)$ correlated best with [Turb], rather than TSS or other measures of suspended particulate load (Figure 3a). At all wavelengths, the relationship between particulate absorption, $[a_d(\lambda)]$, and particulate matter as measured by [Turb] seemed to fall into 2 groups (Figure 3b). Coefficients of determination were higher when regressions were done by group, and individual spectra of diffuse attenuation were better reconstructed from water quality measurements when the particular regression corresponding to the group an individual sample fell in was used to predict the spectrum. Generally, samples in the group with the high slope were from stations far from Ft. Pierce Inlet, with the exception of one sample from Marker 184 and 2 samples from Marker 186. Similarly, samples in the group with the low slope were generally from stations near the Inlet, except for 1 sample from Marker 198. No other measurable factors about the suspended particulate matter enabled prediction of which slope a particular sample would fall in, so that for the general model of diffuse attenuation spectra, the regression on the pooled data has been used. That is, the specific absorption coefficient of suspended particulate matter appears to be spatially variable, but location alone is not a reliable enough predictor to characterize the variability. Some inherent uncertainty will, therefore, be present due to variability in particulate absorption properties.

Regression slopes of $a_d(\lambda)$ against turbidity based on the pooled data from profiles unaffected by discharge of colored water were used to describe the wavelength dependence of the specific absorption of non-algal particulate matter (Figure 4). Similar to previous work (Gallegos in press), the relationship is well described by equation 8b. Estimated parameters in the relationship are σ_{bl}=0.0627 m^{-1} NTU^{-1}, σ_{400}=0.298 m^{-1} NTU^{-1}, and s_d=0.0155 nm^{-1}.

Specific-absorption by phytoplankton chlorophyll, $a^*_{ph}(\lambda)$, was difficult to determine in this work due to relatively low chlorophyll concentrations and predominance of detrital matter in the particulate material. Consequently, individual spectra of $a^*_{ph}(\lambda)$ were noisy (Figure 5). As in previous work (Gallegos et al. 1989, Gallegos in press) there was a high degree of variability in $a^*_{ph}(\lambda)$, which is believed to be of biological origin. Due to the relatively low (for estuaries) chlorophyll concentrations and to the predominance of turbidity encountered here, variability from profile-to-profile in $a^*_{ph}(\lambda)$ is not likely to result in large errors in predicitons. For the model presented here, I used values of $a^*_{ph}(\lambda)$ determined for the Rhode River, MD, because chlorophylls there are higher and, hence, $a^*_{ph}(\lambda)$ is better resolved, and the Rhode River curve seems to pass through the central tendency of the (somewhat noisy) curves measured in the Indian River (Figure 5). Values of $a^*_{ph}(\lambda)$ and $a_w(\lambda)$ are given in Table 1.

As determined by other authors (Bricaud et al. 1981; Gallegos et al. 1989; Cuthbert and Del Giogio 1992), absorption by dissolved yellow matter had a negative exponential dependence on wavelength in the visible region of the spectrum (Figure 6). Given the broad range in color, the $a_y(\lambda)$ is well modeled by equation 7 with s_y=0.016 nm^{-1} (Cuthbert and Del Giorgio 1992). g_{440} can be measured on filtered water with a spectrophotometer or estimated using equation 14. A summary of the modeled optical properties, governing equations, water quality correlate, and parameter values is given in Table 2.

Diffuse attenuation for PAR, K_d(PAR), was calculated as described in equations 10 and 11. Comparison of predicitons against observed values is given in Figure 7. For statistical comparison of predicted and observed K_d(PAR), consideration is restricted to profiles unimpacted by color, due to occurrence of color as a thin layer; vertical non-uniformity in water quality distribution does not meet all assumptions of the theory outlined above, but predictions based on depth-integrated samples appear to be satisfactory (Figure 7, triangles; *see also* Gallegos et al. 1990). Based on aggregate statistics, the model predicts a mean K_d(PAR) of 1.02 m^{-1} and standard deviation of 0.22 m^{-1} in low-color profiles, compared with observed mean and standard deviaiton of 0.92 and 0.18 m^{-1} respectively; the means are not significantly different. Based on paired samples, the model predictions are biased slightly high, with a mean difference (predicted–observed) of 0.096 m^{-1} which is statistically different from 0 ($t=2.63$, $P<0.05$, d.f.=23). The difference is <10% of the observed range (>1 m^{-1}). Furthermore, it would not be correct to assign all of the difference to model error, since the Licor sensor departs from an ideal quantum response at the blue and red ends of the spectrum, which are relative maxima in the diffuse attenuation spectra in coastal waters. Predictions of K_d(PAR) for the upper 0.5 m in highly colored water demonstrate the impact of color on diffuse attenuation (Figure 7, circles); but the degree of scatter is enhanced because of the

extreme color variations in the upper 0.5 m and the difficulty of matching water samples with attenuation profiles over these short distances.

B. Factors Controlling Light Attenuation under Existing Conditions. Three water quality parameters were found to be sufficient to model the spectrum of diffuse attenuation coefficient in the Indian River near Ft. Pierce, FL. The relative importance of each factor can be determined by examining the sensitivity of model predictions of K_d(PAR) to the normal variability and covariability of the water quality constituents (*i.e.* color, chlorophyll, and turbidity). For profiles outside the influence of the colored water plume, this was by a Monte Carlo procedure with the calibrated optical model, in which water quality concentrations were drawn at random from distributions similar to those observed. These values were input into the water quality model, which then calculated K_d(PAR) and the 20% penetration depth, Z_{20}(PAR).

Statistical characteristics of the water quality distributions (mean, standard deviation, and simple correlation coefficients, r) are given in Table 3. All water quality variables were drawn from normal distributions truncated to limits observed in measured data. The sensitivity to each water quality parameter was evaluated by holding all other parameters constant at their mean and allowing the selected parameter to vary according to its assumed distribution. Mean, standard deviation, minimum, and maximum K_d(PAR) and Z_{20}(PAR) are reported in Table 4 for each scenario. Sensitivity was evaluated as the standard deviation of the predictions relative to the base run condition with all parameters variable. Evaluations are based on 200 realizations for each simulation.

The predicted mean Z_{20}(PAR) for conditions unaffected by color discharge (=1.38 m, Table 4) was very close to the value of 1.37 m determined for the seagrass bed at Marker 198 in August 1993 (*see* Part II); predicted standard deviation was 0.34 m. For K_d(PAR) the predicted mean and standard deviation with all water quality parameters variable was 1.23 and 0.28 m^{-1}, respectively. Nearly all of the variability (89-91 percent) was due to the range of turbidity encountered. Variations in chlorophyll and color alone could account for no more than 15 percent of the variability in the predicted coefficients. (The percentages can sum to >100 because of the assumed covariability between water quality concentrations). Thus, at Marker 198, turbidity is the primary factor governing changes in attenuation of PAR and consequent changes in seagrass survival depths.

A similar analysis for the seagrass bed near Marker 184 was not as straightforward, because we could not sample directly over the grass bed in the vessel available. I estimated existing color conditions over the grass bed 2 ways. Using the optical model with chlorophyll and turbidity set at

their average values for non-impacted conditions, color was varied until predicted Z_{20}(PAR) matched the distribution observed in August 1993, i.e. 87 cm. The average color concentration determined in this was was 65 Pt. units. Alternatively, I assumed that the grass bed was either inundated by the color plume, which from observed data, varied from 70–90 Pt. units, or was covered by water with color from 5-8 Pt.units, with chlorophyll and turbidity like that assumed previously (Table 3). The relative proportion of cases drawn from the 2 color populations was varied until the predicted Z_{20}(PAR) matched the observed depth of seagrasses near Marker 184 in August 1993. The proportion of coverage by highly colored water that produced the best match was 75%.

With these conditions defining the base run, sensitivity to variations in color, chlorophyll, and turbidity were tested as before, by allowing the parameter of interest to vary as in the base run, and holding the other 2 constant (Table 5). With color as the only varying constituent, predicted standard deviations of K_d(PAR) and Z_{20}(PAR) were, respectively, 85 and 100 percent of the base run simulation. Predicted distributions of K_d(PAR) and Z_{20}(PAR) were bimodal when color alone was varied. Sensitivity to chlorophyll and turbidity at Marker 184 was tested by holding color constant at 65 Pt. units and varying chlorophyll and turbidity as in the base run simulation. At the higher color, sensitivity to chlorophyll was even less than at Marker 198, producing standard deviations in predicted K_d(PAR) and Z_{20}(PAR) $\leq$5 percent of base run conditions. Variability in turbidity alone produced standard deviations in K_d(PAR) and Z_{20}(PAR) approximately 50 percent of base run. With the higher background color, the minimum K_d(PAR) was 1.42 m^{-1} when turbidity alone was varied, compared with 0.68 m^{-1} when color also varied between 2 populations. Thus at Marker 184, color and turbidity jointly control attenuation, with the effect of intermittent inundation by highly colored water being to produce 2 discrete distributions of attenuation, and simultaneous variation in turbidity being to fill in gaps between the 2 distributions and to slightly extend the overall range [*see* Table 5, Min. and Max, K_d(PAR)].

C. Contours of 20% Penetration Depth. The optical model was used to determine water quality concentrations that would permit penetration of 20% of surface irradiance to a range of depths. For this analysis chlorophyll was held constant at 4 $\mu g\ L^{-1}$ because of the relative insensitivity to that parameter at these locations. A range of color concentrations was selected likely to span those encountered, and at each color, the turbidity was determined that would predict values of Z_{20}(PAR) ranging from 0.75–2.5 m at 0.25m intervals (Figure 8a). Contours are plotted on logarithmic axes so that equidistant movements along either axis represent constant proportional changes in concentrations, regardless of units of measurement. Furthermore, management actions are generally planned in terms of percentage reductions in loadings.

Average concentrations of Color=7.9 Pt. units and Turbidity=3.2 NTU locates Marker 198 between the 1.25 and 1.5 m contours (Figure 8a, X), similar to observed seagrass distributions (*see* Part II). As indicated by the analysis in B above, the contours in Figure 8a confirm that Marker 198 is in a region in which attenuation is governed almost solely by turbidity. To attain conditions for seagrass growth to 2 m at Marker 198 it would be necessary to reduce turbidity to <2 NTU, with only modest reduction in color to ≈5 Pt. units.

At Marker 184 it was necessary to infer an average color concentration of ≈65 Pt. units from the observed depth limit of 0.87 m. That color concentration places Marker 184 in a region in which attenuation is jointly governed by color and turbidity (Figure 8a), as was also shown above. The depth distribution of seagrasses at Marker 184 could be made to equal that at Marker 198 by reduction of color to 7.9 Pt. units (horizontal movement in Figure 8a) or by simultaneous reduction of average color to ≈30 Pt. units and turbidity to ≈2 NTU (diagonal movement in Figure 8a). The latter action assumes that turbidity is controllable.

The sensitivity to a third variable, i.e. chlorophyll, can be examined by plotting a single Z_{20}(PAR) depth contour at a range of different chlorophyll concentrations (Figure 8b). For this analysis, I chose the Z_{20}(PAR)=1.5 m, because that is close to the maximum depth distribution measured at Marker 198. An interpretation of the figure is that as chlorophyll increases, the contours show the reduction in turbidity and color that would be necessary to maintain seagrass growth to 1.5 m.

D. Analysis of alternative color change scenarios. The plume of colored water discharged at Taylor Creek was observed to form a thin surface lense which sometimes moved across the ICW channel and out the Ft. Pierce Inlet, and sometimes northward along the west shore, covering the seagrass bed at the site. A well-defined, easily visible front separated Taylor Creek water from inlet or lagoonal water not affected by Taylor Creek. Color concentration generally ranged from 70–90 Pt. units in the surface water leaving Taylor Creek, and 5–8 Pt. units across the front in water not affected by Taylor Creek discharge. The analysis of alternative scenarios involving discharge from Taylor Creek, therefore, proceeded on the premise that the seagrass bed is inundated either by the color plume leaving Taylor Creek or covered by water of normal lagoonal quality. Scenarios investigated included the effect of alteration of the frequency of inundation, and of changes in the color concentration of the inundating plume, holding frequency of coverage constant.

As described in B above, a Monte Carlo analysis was conducted to investigate the alternative scenarios. Color of the water covering the seagrass bed was drawn from one of 2 populations having limits given above. When all of the color values were drawn from the low-color population

(i.e. 0 percent inundation by color plume), predicted mean Z_{20}(PAR) was 1.39 m, similar to that observed at Marker 198 in August 1993 (Figure 9a). Increasing the percent inundation (i.e. the percentage of color values drawn from the high color population) resulted in steady reduction in Z_{20}(PAR). Predicted Z_{20}(PAR) for 100 percent coverage was ≈79 cm; the percent inundation providing the closest match with existing conditions at the Taylor Creek seagrass bed was 75% (predicted Z_{20}(PAR)=90 cm, Figure 9b).

The 75 percent frequency of inundation was used as the basis for investigating the effect of reducing color concentration in the discharge water (Figure 9b). The model predicted that each reduction of color in the discharge water would result in increases in Z_{20}(PAR). Predicted Z_{20}(PAR) for a reduction in the range of color in discharge water to 10–30 Pt. units was 1.22 m, or 68 percent of the way toward recovery to non-impacted conditions.

V. DISCUSSION

A. Limitations. As discussed above under Model Calibration, there was a slight tendency for the optical model to overestimate K_d(PAR) relative to observed values. When evaluation of the model is extended to include all 40 profiles for which we have both water quality samples and PAR profiles, the mean residual falls to 0.075 m^{-1}. The standard deviation of the residuals is 0.16 m^{-1}, which provides an estimate of how well we should expect individual estimates to agree when comparing predictions with observtions on other data sets. The mean K_d(PAR) over all 40 profiles was 1.067 m^{-1}, so that ca. 15% represents a reasonable coefficient of variation. It is important to note that observed K_d(PAR) also contain random error, which contributes to some of the uncertainty.

The Monte Carlo analysis of K_d(PAR) and Z_{20}(PAR) using observed distributions of water quality variables predicted a maximum depth distribution for Halodule wrightii and Syringodium filiforme at Marker 198 of 1.37 m, which was nearly identical to that observed in August 1993. The highest turbidities were observed at that site in the May 1993 field trip. Excluding the May 1993 trip, average water quality concentrations for low-color profiles were color=7.77 Pt. units, chlorophyll=3.69 μg L^{-1}, turbidity=3.00 NTU, μ_0=0.82. Insertion of these values in the optical model predicts Z_{20}(PAR)=1.48 m, again nearly identical to that observed in March 1993. The agreement is encouraging for the general use of the model in the Lagoon. If the model is indeed biased high, then the appropriate ecological compensation light level in relation to measured K_d(PAR) would be closer to 22% of surface light. This is well within the uncertainty determined from previous field surveys (*see* Part II).

B. Recommendations. The existing water quality monitoring programs in the Indian River Lagoon provide the potential for widespread application of the model. Although every effort was made in this study to conform to standard methods of analysis as outlined in the RQAP submitted to the Florida Department of Environmental Regulation, differences in manufacturers' instrumentation, lot differences in commercially supplied standards, and subjective differences among investigators, in e.g. visual color determinations, provide the potential for systematic differences in estimated water quality parameters between those used in calibration of the model and those determined in routine monitoring programs. As described in Appendix A (**Model Documentation**), coefficients were included in the model to easily adjust for any such analytical differences. A workshop to compare water quality analyses on common samples is advisable to reveal if any such modifications are necessary.

Bibliography

Bowling, L. C., M. S. Steane and P. A. Tyler. 1986. The spectral distribution and attenuation of underwater irradiance in Tasmanian inland waters. Freshwater Biology 16:313-335.

Bricaud, A., A. Morel and L. Prieur. 1981. Absorption by dissolved organic matter of the sea (yellow substance) in the UV and visible domains. Limnology and Oceanography 26:43-53.

Cuthbert, I. D. and P. del Giorgio. 1991. Toward a standard method of measuring color in freshwater. Limnology and Oceanography 37:1319-1326.

Dennison, W. C., R. J. Orth, K. A. Moore, J. C. Stevenson, V. Carter, S. Kollar, P. W. Bergstrom and R. A. Batiuk. 1993. Assessing water quality with submersed aquatic vegetation. BioScience 43:86-94.

Gallegos, C. L. 1994. Refining habitat requirements of submersed aquatic vegetation: role of optical models. Estuaries, in press.

Gallegos, C. L., D. L. Correll and J. W. Pierce. 1990. Modeling spectral diffuse attenuation, absorption, and scattering coefficients in a turbid estuary. Limnology and Oceanography 35:1486-1502.

Gordon, H. R. 1991. Absorption and scattering estimates from irradiance measurements: Monte Carlo simulations. Limnology and Oceanography 36:769-776.

Jeffrey, S. W., and G. F. Humphrey. 1975. New spectrophotometric equation for determining chlorophyll *a*, *b*, c^1, and c^2 in higher plants, algae, and natural phytoplankton. Biochem. Physiol. Pflanz. 167: 191-194.

Kenworthy, W. J. 1992. Protecting fish and wildlife habitat through an understanding of the minimum light requirements of subtropical-tropical seagrasses of the southeastern United States and Caribbean Basin. PhD. Dissertation, North Carolina State University, Raleigh, NC. 258 pp.

Kenworthy W. J. and D. E. Haunert. 1991. The light requirements of seagrasses: proceedings of a workshop to examine the capability of water quality criteria, standards and monitoring programs to protect seagrasses. NOAA Technical Memorandum NMFS-SEFC-287.

Kirk, J. T. O. 1981. Monte Carlo study of the nature of the underwater light field in, and the

relationships between optical properties of, turbid, yellow waters. Austrialian Journal of Marine and Freshwater Research 32:517-532.

Kirk, J. T. O. 1984. Dependence of relationship between inherent and apparent optical properties of water on solar altitude. Limnology and Oceanography 29:350-356.

Kirk, J. T. O. 1991. Volume scattering function, average cosines, and the underwater light field. Limnology and Oceanography 36:455-467.

Maske, H. and H. Haardt. 1987. Quantitative in vivo absorption spectra of phytoplankton: Detrital absorption and comparison with fluorescence excitation spectra. Limnology and Oceanography 32:620-633.

Morel, A. and B. Gentili. 1991. Diffuse reflectance of oceanic waters: Its dependence on Sun angle as influenced by the molecular scattering contribution. Applied Optics 30:4427-4438.

Morel, A. and R. C. Smith. 1982. Terminology and units in optical oceanography. Marine Geodesy 5:335-349.

Phillips, D. M. and J. T. O. Kirk. 1984. Study of the spectral variation of absorption and scattering in some Australian coastal waters. Austrialian Journal of Marine and Freshwater Research 35:635-644.

Preisendorfer, R. 1976. Hydrologic optics. NOAA, Washington, D. C.

Prieur, L. and S. Sathyendranath. 1981. An optical classification of coastal and oceanic waters based on the specific spectral absorption curves of phytoplankton pigments, dissolved organic matter, and other particulate materials. Limnology and Oceanography 26:671-689.

Roessler, C. S., M. J. Perry and K. L. Carder. 1989. Modeling in situ phytoplankton absorption from total absorption spectra in productive inland marine waters. Limnology and Oceanography 34:1510-1523.

Smith, R. C. and K. S. Baker. 1981. Optical properties of the clearest natural waters. Appl. Opt. 20: 177-184.

Smith, W. O., Jr. 1982. The relative importance of chlorophyll, dissolved and particulate material, and seawater to the vertical extinction of light. Estuarine, Coastal and Shelf Science 15:459-465.

Vant, W. N. 1990. Causes of light attenuation in nine New Zealand estuaries. Estuarine, Coastal and Shelf Science 31:125-137.

Weast, R. C. 1977. Handbook of chemistry and physics. Chemical Rubber Co., p.

Weidemann, A. D. and T. T. Bannister. 1986. Absorption and scattering coefficients in Irondequoit Bay. Limnology and Oceanography 31:567-583.

Witte, W. G. and others. 1982. Influence of dissolved organic materials on turbid water optical properties and remote-sensing reflectance. Journal of Geophysical Research 87:441-446.

Table 1. Tabulated values of absorption coefficient of pure water, a_w, and of the chlorophyll-specific absorption coefficient of phytoplankton, a^*_{ph}, as a function of wavelength, λ (nm). Units of a_w are m^{-1}; units of a^*_{ph} are m^{-2} (mg Chl a)$^{-1}$. $a_w(\lambda)$ from Smith and Baker (1981).

λ	a_w	a^*_{ph}	λ	a_w	a^*_{ph}	λ	a_w	a^*_{ph}	λ	a_w	a^*_{ph}
400	.0171	.0365	**475**	.0166	.0330	**550**	.0638	.0099	**625**	.3140	.0096
405	.0167	.0385	**480**	.0176	.0316	**555**	.0637	.0089	**630**	.3190	.0097
410	.0162	.0414	**485**	.0186	.0308	**560**	.0708	.0081	**635**	.3240	.0094
415	.0160	.0449	**490**	.0196	.0303	**565**	.0754	.0075	**640**	.3290	.0091
420	.0158	.0464	**495**	.0227	.0290	**570**	.0799	.0075	**645**	.3390	.0088
425	.0151	.0486	**500**	.0257	.0362	**575**	.0940	.0075	**650**	.3490	.0089
430	.0144	.0509	**505**	.0307	.0234	**580**	.1080	.0072	**655**	.3745	.0099
435	.0145	.0519	**510**	.0357	.0213	**585**	.1325	.0075	**660**	.4000	.0131
440	.0145	.0499	**515**	.0417	.0185	**590**	.1570	.0075	**665**	.4150	.0169
445	.0145	.0461	**520**	.0477	.0168	**595**	.2005	.0072	**670**	.4300	.0210
450	.0145	.0419	**525**	.0492	.0149	**600**	.2440	.0073	**675**	.4440	.0212
455	.0151	.0398	**530**	.0507	.0140	**605**	.3665	.0075	**680**	.4500	.0187
460	.0156	.0387	**535**	.0533	.0127	**610**	.2890	.0080	**685**	.4750	.0146
465	.0156	.0373	**540**	.0558	.0117	**615**	.2990	.0088	**690**	.5000	.0100
470	.0156	.0355	**545**	.0598	.0109	**620**	.3090	.0094	**695**	.5750	.0052
									700	.6500	.0028

Table 2. Summary of optical properties, governing equation in text, water quality correlate, and calibrated parameter values for optical model of diffuse attenuation spectrum in Indian River near Ft. Pierce, FL.

Quantity	Equation	Water Quality Input	Parameter(s)	Value(s)
a_w	N/A	N/A	N/A	*See Table 1*
a_y	7	Color	g_{440}; s_y	0.074*Color; 0.016
a_{ph}	9	Chlorophyll *a*	a^*_{ph}	*See Table 1*
a_d	8	Turbidity	σ_{bl}; σ_{400}; s_d	0.0627; 0.298; 0.0155
a_t	5	N/A	N/A	N/A
b	6	Turbidity	N/A	Measured Input
K_d	3,4	N/A	μ_0	(0.74–0.98), diurnally and seasonally variable

Table 3. Statistical attributes of optical water quality variables measured at station 198 and other stations (184, 186, 172, Inlet) when not covered by colored water plume. These properties were used in a Monte Carlo simulation with the calibrated optical model to assess the factors controling attenuation in unimpacted locations.

	Color (Pt. Units)	Chlorophyll ($\mu g\ L^{-1}$)	Turbidity (NTU)
Mean	7.90	4.07	3.73
Std. Dev.	3.13	1.78	1.68
Correlation Coef.			
Chlorophyll	0.495	°	°
Turbidity	0.213	0.740	°

Table 4. Sensitivity analysis of optical model predictions of diffuse attenuation coefficient for PAR, K_d(PAR), and 20% penetration depth, Z_{20}(PAR). For base run conditions (**All Variable**) water quality concentrations were drawn at random according to distributions and correlations given in Table 3. Sensitivity of model predictions to variations in color, chlorophyll, and turbidity was determined by allowing the parameter in bold type to vary as specified in Table 3, while holding the other 2 concentrations constant. Units of K_d(PAR) are m^{-1}, and units of Z_{20}(PAR) are m.

MARKER 198 SOUTH

	All Variable		**Color**		**Chlorophyll**		**Turbidity**	
	K_d(PAR)	Z_{20}(PAR)	K_d(PAR)	Z_{20}(PAR)	K_d(PAR)	Z_{20}(PAR)	K_d(PAR)	Z_{20}(PAR)
Mean	1.23	1.38	1.17	1.38	1.17	1.38	1.19	1.40
Std. Dev.	0.28	0.34	0.04	0.05	0.03	0.03	0.25	0.31
Min.	0.62	0.82	1.08	1.27	1.07	1.30	0.71	0.81
Max.	1.96	2.59	1.27	1.49	1.25	1.48	1.98	2.27
% of Base Run	100	100	14.3	14.7	10.7	8.8	89.3	91.2

Table 5. As Table 4, except for the base run simulation, color was drawn from a distribution that varied uniformly from 5–8 Pt. units 25% of the time, and from 70–90 Pt. units 75% of the time. To test sensitivity to chlorophyll and turbidity, color was held constant at 65 Pt. units.

MARKER 184

	All Variable		**Color**		**Chlorophyll**		**Turbidity**	
	K_d(PAR)	Z_{20}(PAR)	K_d(PAR)	Z_{20}(PAR)	K_d(PAR)	Z_{20}(PAR)	K_d(PAR)	Z_{20}(PAR)
Mean	1.84	0.91	1.76	0.96	1.85	0.87	1.87	0.87
Std. Dev.	0.40	0.23	0.34	0.23	0.02	0.01	0.23	0.11
Min.	0.68	0.60	1.10	0.79	1.82	0.84	1.42	0.60
Max.	2.68	2.37	2.10	1.39	1.92	0.89	2.68	1.14
% of Base Run	100	100	85	100	5	2.9	57.5	47.8

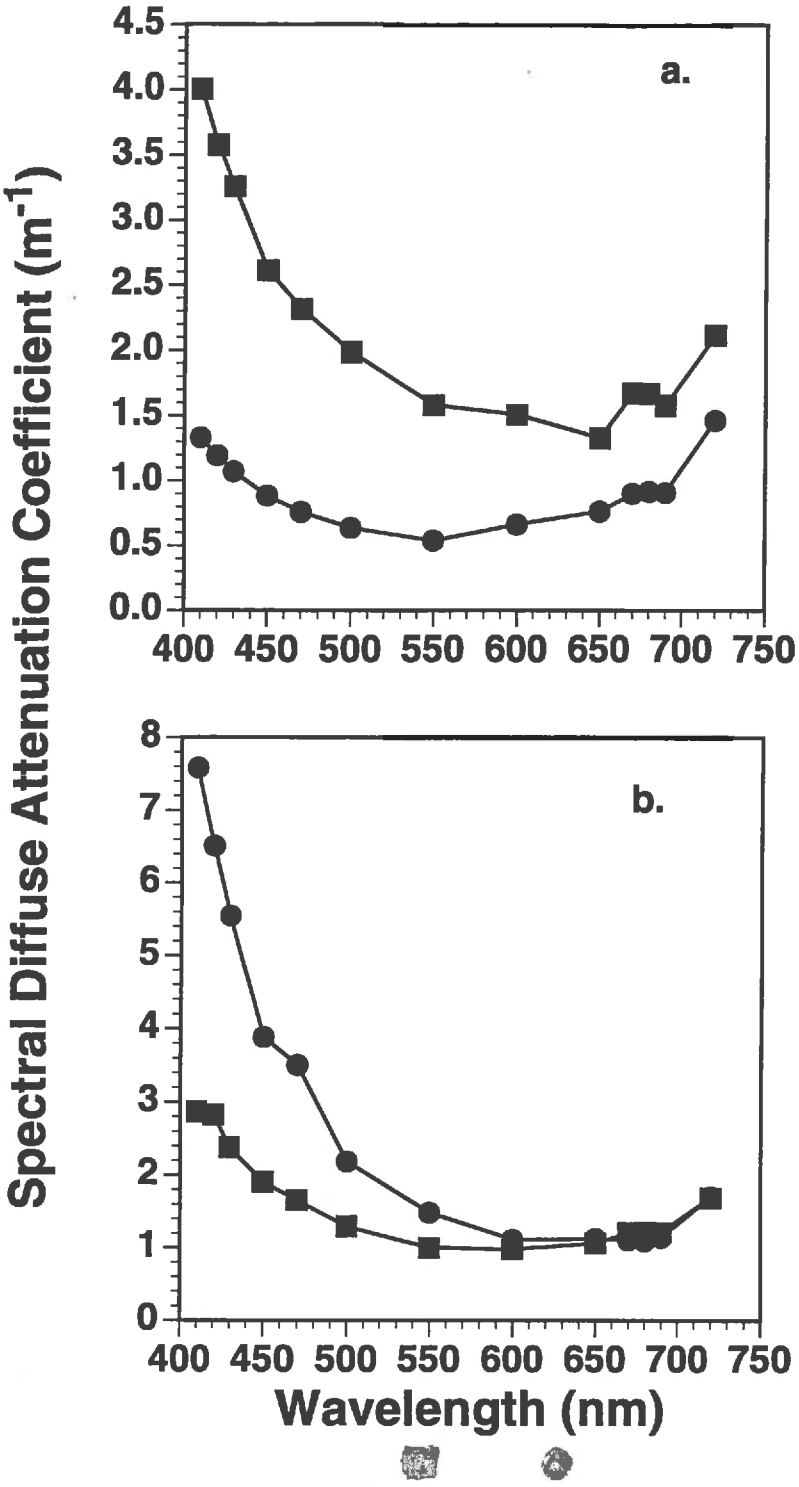

Figure 1. a—Examples of diffuse attenuation spectra for stations not impacted by colored water discharge, having (B) high and (J) low turbidity. b—Effect of color occurring as a thin surface layer on calculated diffuse attenuation coefficients at station C-25 in Taylor Creek: (B) calculated based on measurements from the surface to the bottom. (J) calculated using measurements from the surface to 0.5 m.

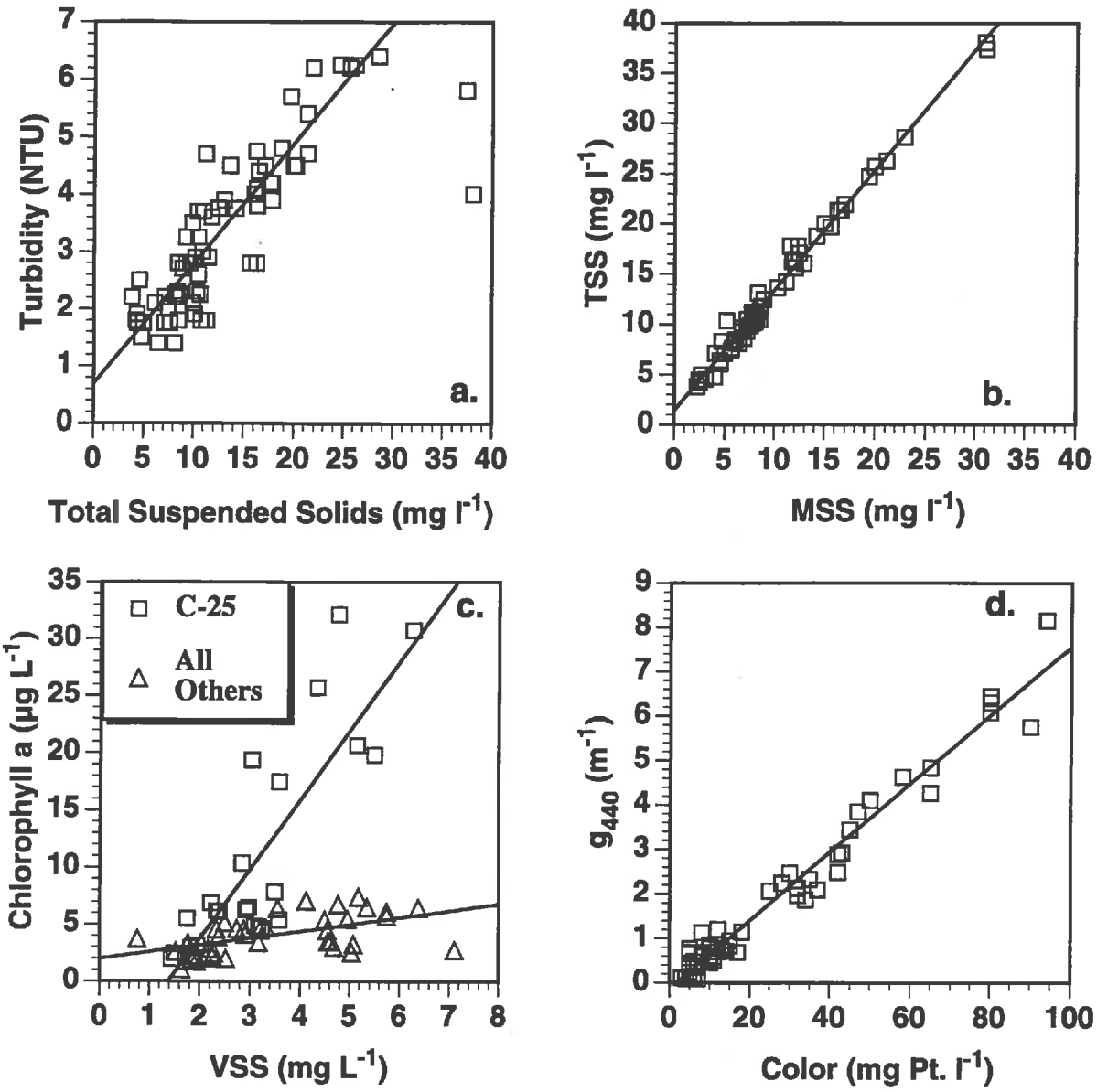

Figure 2. Relationships amongst water quality variables in the Indian River Lagoon.

a—Turbidity as a function of total suspended solids (TSS); 2 outliers at TSS>30 mg L^{-1} omitted from regression line. b—TSS as a function of mineral suspended solids (MSS). c—Chlorophyll a concentration as a function of volatile suspended solids (VSS, =TSS-MSS) at Station (□) C-25 and (△) at all other stations. Phytoplankton from upstream freshwater sources appears to be the source of the high chlorophyll concentrations at C-25. d—relationship between absorption coefficient at 440 nm, g_{440}, and dissolved color measured by the visual comparison method.

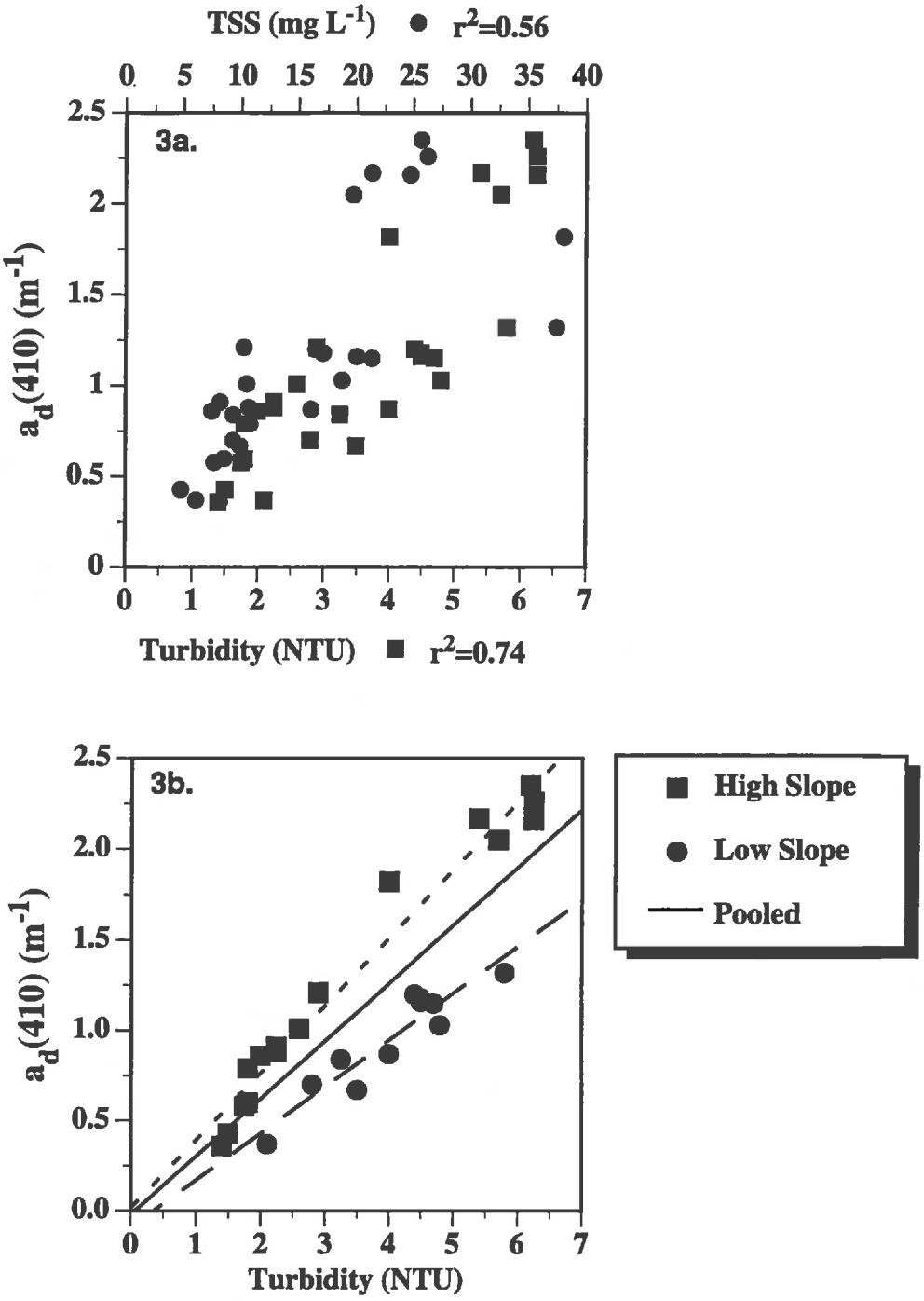

Figure 3. a—Regressions of absorption by non-algal particulate matter against (●) total suspended solids (TSS), and against (■) turbidity. Regressions at all wavelengths had higher coefficients of determination with turbidity as independent variable. b—Specific absorption by non-algal particulate matter appeared to 2 groups with high (■) and low (●) slopes, station location was inadequate predictor of group assignment. Consequently, regressions on pooled data were used to describe specific absorption as a function of wavelength.

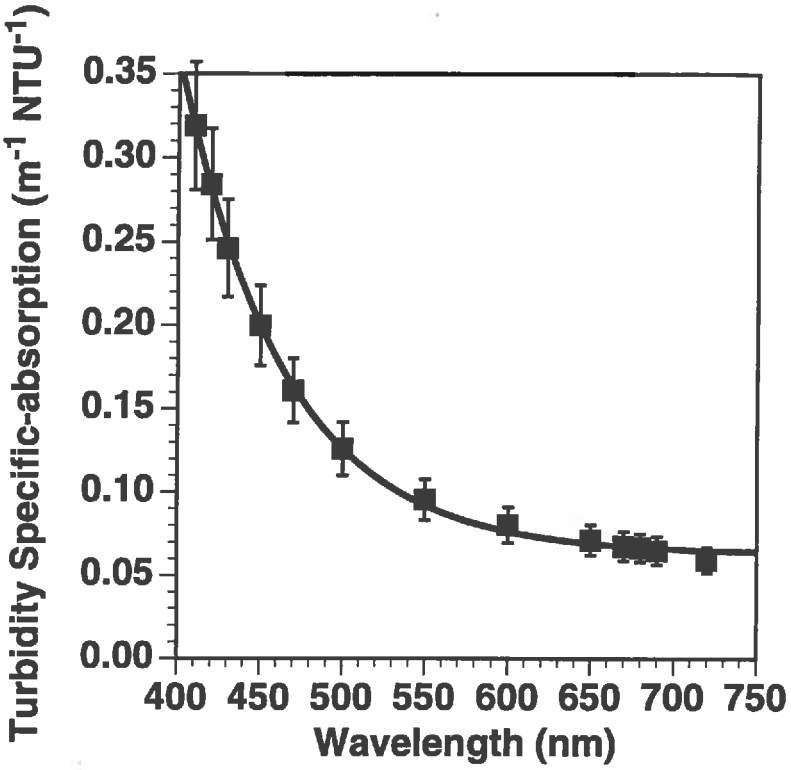

Figure 4. Specific absorption coefficient (±1 s.e.) of turbidity as a function of wavelength for profiles unaffected by colored water discharge. Specific absorption coefficient is the slope of a regression of $a_p(\lambda)$ *versus* turbidity. Fitted curve is equation 8b with parameters σ_{bl}=0.0627, σ_{400}=0.298, and s_d=0.0155. Units of σ_{bl} and σ_{400} are m^{-1} NTU^{-1}; units of s_d are nm^{-1}.

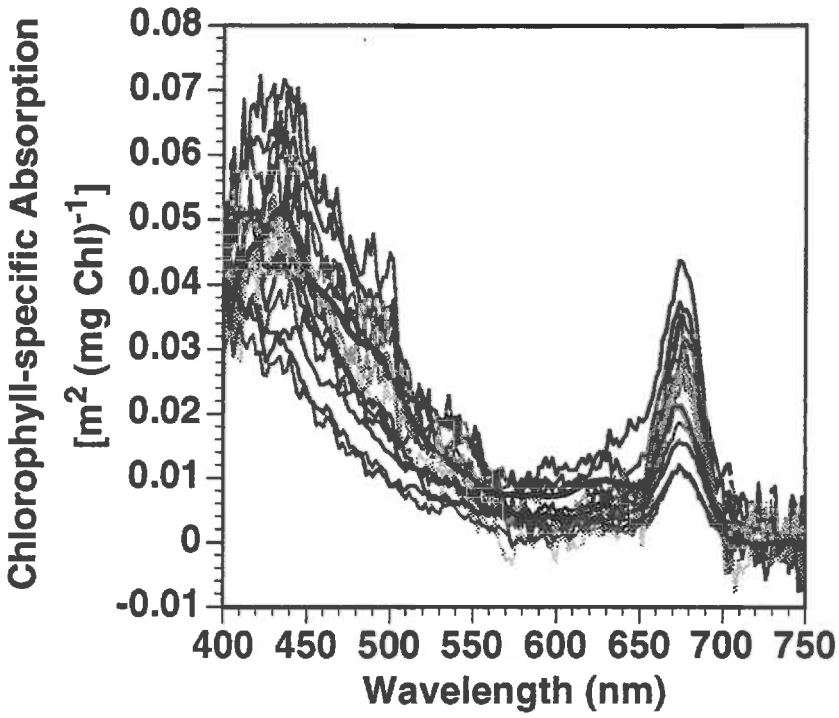

Figure 5. Absorption by phytoplankton normalized to chlorophyll concentration as a function of wavelength for 17 stations on the Indian River, FL (•). Solid curve is mean determined on samples from Rhode River, MD in which chlorophyll concentration exceeded 30 $\mu g\ L^{-1}$, and in which chlorophyll-specific absorption is more easily resolved from non-algal particulate matter. Values from the solid curve are used in optical model (*see text*).

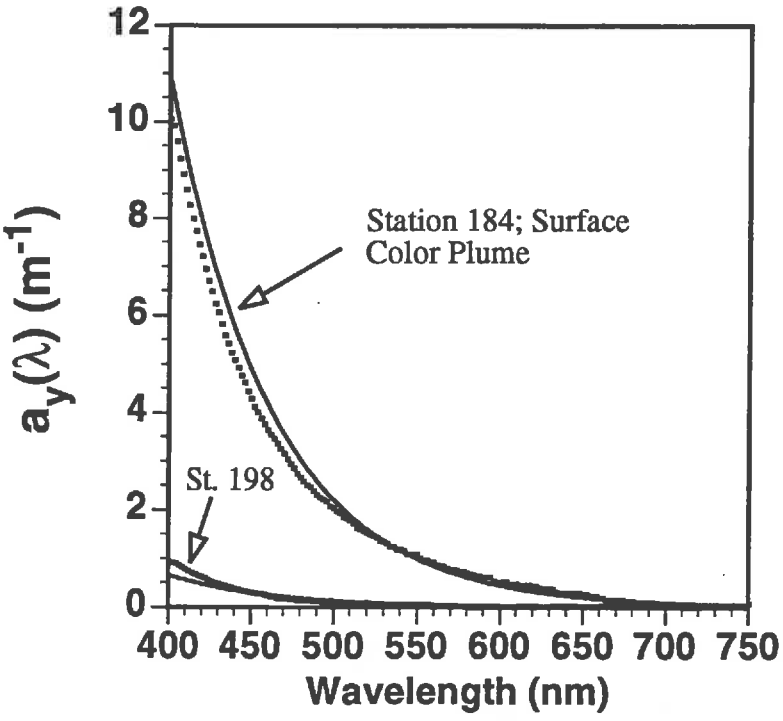

Figure 6. Absorption by dissolved matter [$a_y(\lambda)$] measured in March 1993 at Station 184, which was within the surface plume of colored water discharged from Taylor Creek, and at Station 198, south of Ft. Pierce Inlet and unimpacted by colored water discharge. Symbols are measurements, and lines are model prediction based on $a_y(\lambda)=g_{440}$*exp[(–0.016*(λ-440)].

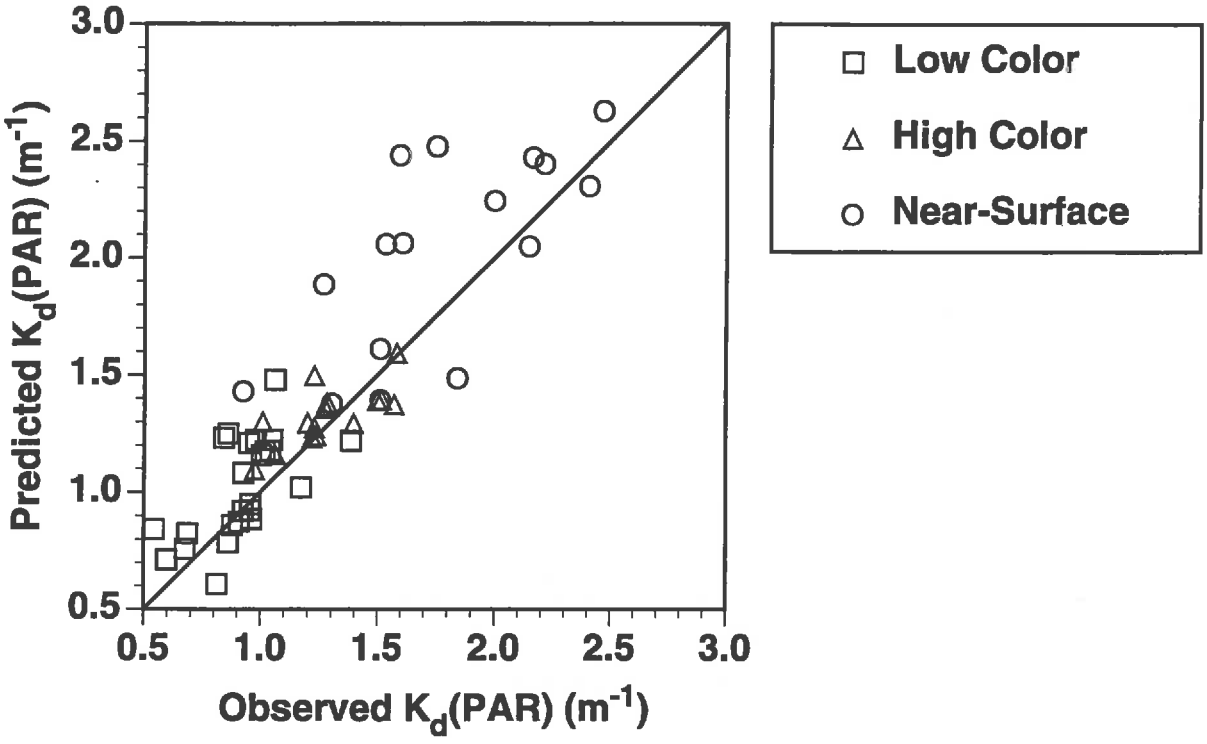

Figure 7. Comparison of observed diffuse attenuation for PAR with calculations with the optical model. Samples designated Low Color (□) were from Station 198, 186, 172, and 184 when not influenced by Taylor Creek outflow. Samples designated High Color (Δ) were from C-25 and 184 when covered by surface color plume from Taylor Creek. Calculations based measurements from immediately subsurface to bottom. Near-surface samples were from the same profiles as High Color, with calculations based on water quality and PAR measurements within the top 0.5 m.

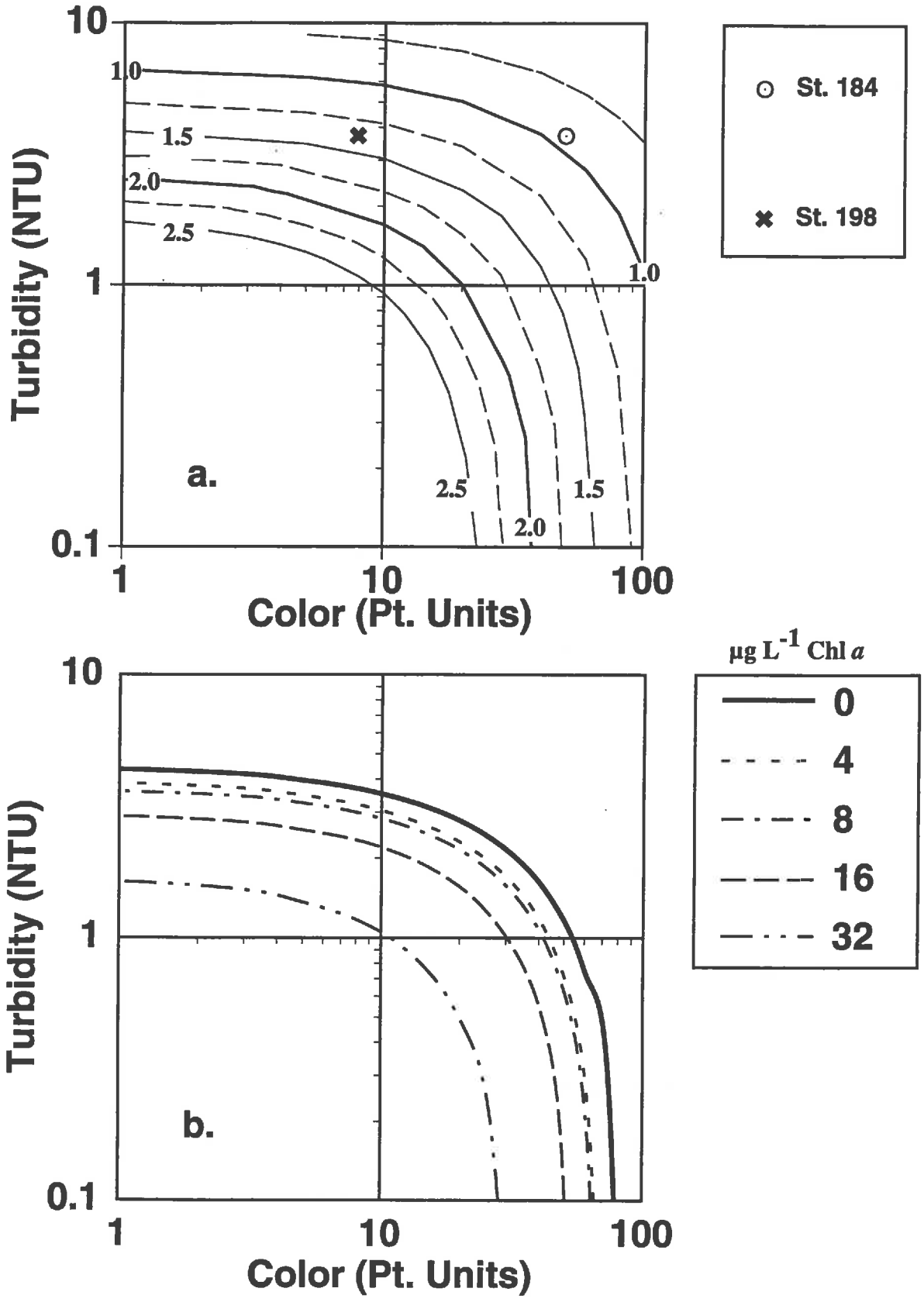

Figure 8. a—Contours of Z_{20}(PAR) calculated by the optical model as a function of color and turbidity. Numbers on the contour lines are 20% penetration depths in meters. Chl and μ_0 were held constant at 4 µg L^{-1} and 0.92, respectively. b—Contours of color and turbidity values that predict Z20(PAR)=1.5 m for different values of chlorophyll given in the legend.

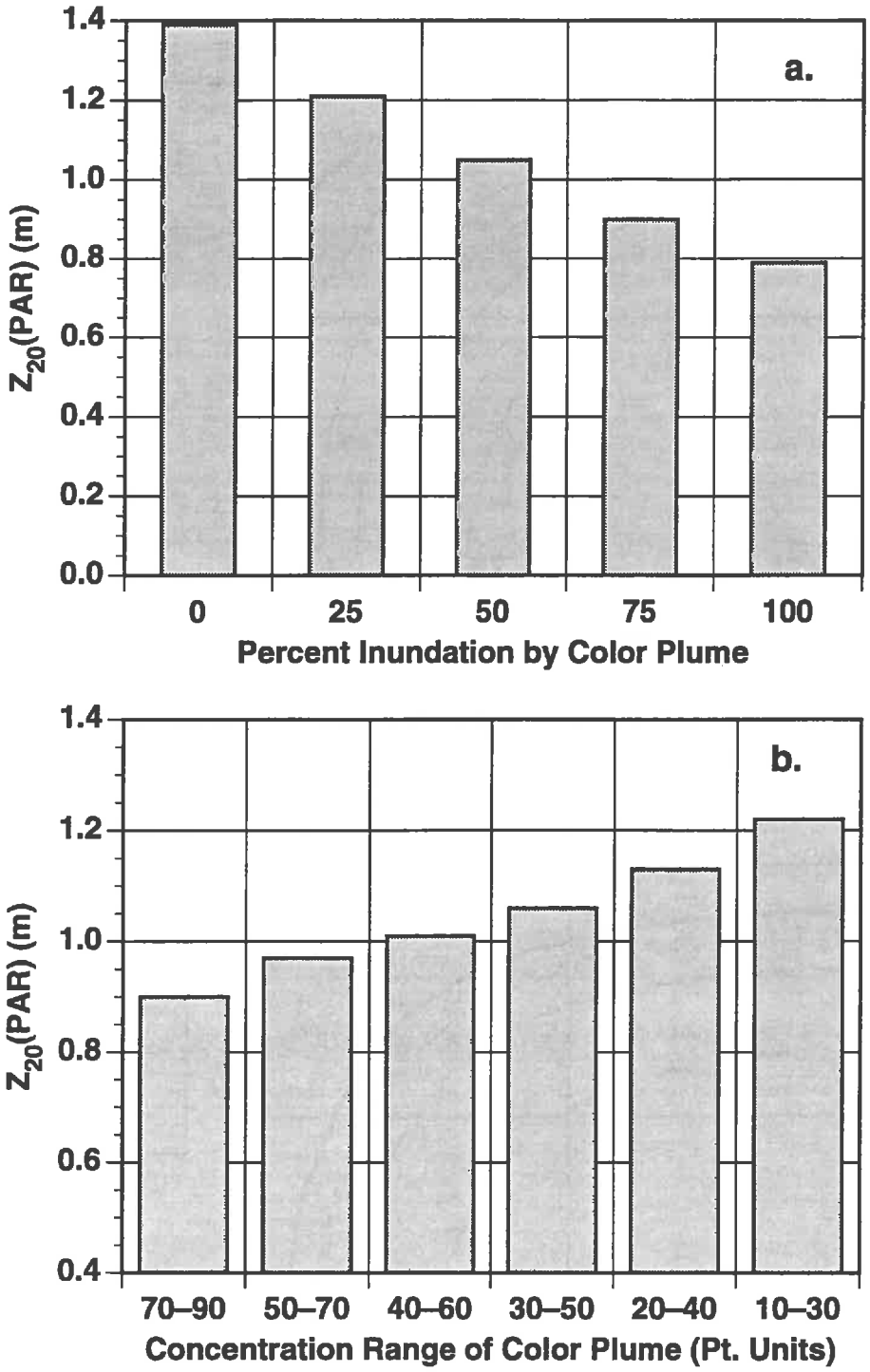

Figure 9. Analysis of alternative color scenarios. a—Effect of variation in frequency of inundation by color plume, having concentration between 70–90 Pt. units, and 5–8 Pt. units when not inundated, on 20% PAR penetration depth. b—Effect of variation in color concentration of discharge plume on 20% PAR penetration depth, assuming seagrass bed is covered by plume 75% of the time.

Appendix A. MODEL DOCUMENTATION

The model for computing spectral diffuse attenuation coefficients and for integrating the underwater spectrum to compute K_d(PAR), the diffuse attenuation for photosynthetically active radiation (PAR), is supplied as a Lotus 123 for IBM compatible PC and as a Microsoft Excel 3.0 for Macintosh spreadsheet. The latter was the development medium. This appendix describes the use of the model and documents the algorithms. Equation, table, and figure numbers refer to the main text of the final report.

There are 5 required user inputs: (1) the color in Pt. units in cell C3; (2) the chlorophyll concentration in $\mu g\ L^{-1}$ in cell D3; the turbidity in NTU in cell E3; (4) the cosine of the refracted solar zenith angle (μ_0, dimensionless) in cell F3; and the water depth in m in cell G3. Appropriate headings are given above each entry location. Values of μ_0 for the location of Marker 184 are given in Table A1; these values are averages over the time period 10:00 A.M. to 2:00 P.M. standard time. A Lotus 123 spreadsheet, called MUZERO.WKS for finer time resolution is also provided. Instructions for its use appear as text in cells B1–B10.

The final outputs of the model are K_d(PAR) (cell D6), the 20% penetration depth, i.e. Z_{20}(PAR) (cell E6), and in cell F6, the percent of surface irradiance remaining at the reference depth. Appropriate headings for these outputs are given in the row immediately above the outputs. In the Microsoft Excel 3.0 version, the outputs are in bold type and red color.

Special attention must be given to the value entered for the reference depth in cell G3. As depth in the water column increases, energy in wavebands for which diffuse attenuation is highest become progressively reduced; i.e. the remaining light becomes skewed to the region of the spectrum in which K_d is minimal. As depth increases, most of the PAR falls in wavebands in which K_d is minimal, hence calculated K_d(PAR) decreases.

The value of depth entered in G3, therefore, depends on the goal of the analysis. If it is

desired to compare a model prediction of K_d(PAR) with a specific field profile of PAR, then water depth of the field profile should be used. If it is desired to determine, for a given water quality combination, the average percentage of surface light reaching the depth limit of a particular grass bed, then the depth limit of interest should be entered. If the desired estimate is the 20 percent penetration depth predicted for a given combination of water quality variables, then the depth entered in G3 should be adjusted until it matches the predicted value output in cell E6.

A series of coefficients are given in cells C8–E9 that are can be adjusted should it become necessary. These are slopes and intercepts that apply linear correction to the water quality concentrations prior to multiplication by their specific absorption and scattering coefficients. Presently, these slopes are 1.0 and offsets 0.0 for chlorophyll and turbidity. The coefficient 0.074 in cell C8 converts color measurements in Pt. units to g_{440} according to equation 14 (Figure 2d). If it is ever determined that there is a linear bias or offset between the data used to calibrate the model and that measured by the user, these coefficients may be adjusted as needed to allow the users to input their own data without recalibrating the model. The coefficients 0.425 and 0.190 in cells F8 and F9 are, respectively, g_1 and g_2 of equation 4.

The main body of the calculations is carried out in 9 columns extending below row 11. Column A contains wavelength in 5 nm intervals from 400–750 nm. Only values from 400–700 nm are used in PAR calculations. The additional wavelengths are included for comparison with more complete profiles of spectral diffuse attenuation coefficient extending into the near infrared (i.e. up to 720 nm).

Column B contains the absorption spectrum of pure water taken from Smith and Baker (1981). Values at odd multiples of 5 nm were determined by linear interpolation of the original data, which were given in 10 nm intervals.

Column C calculates the specific absorption coefficient of dissolved organic matter, i.e. color. The formula implements the right hand side of equation 7, except that multiplication by g_{440}

is done in column F. A spectral slope of 0.016 nm^{-1} is used, as suggested by Cuthbert and Del Giorgio (1992) for humic-stained waters.

Column D contains the chlorophyll-specific absorption coefficient of phytoplankton, $a^*_{ph}(\lambda)$. These values are given along with absorption coefficient of water in Table 1.

Column E calculates the absorption due to non-algal particulate matter according to equations 8a-b. The spreadsheet formula is

($E$3*$E$8+$E$9)*(0.0627+0.298*EXP(-0.0155*(A12-400))),

where ($E$3*$E$8+$E$9) is turbidity (E3) corrected for any bias or offset in E8 and E9, 0.0627=σ_{bl}, 0.298=σ_{400}, 0.0155=s_d, and A12=λ.

Column F calculates total absorption coefficient according to Equation 5. The spreadsheet formula is

B12+C12*($C$8*$C$3+$C$9)+D12*($D$3*$D$8+$D$9)+E12,

where B12=a_w, C12 is the specific absorption due to dissolved matter, ($C$8*$C$3+$C$9) converts color to g_{440}, D12=$a^*_{ph}(\lambda)$, ($D$3*$D$8+$D$9) chlorophyll is in cell D3 and multiplication by D8 and addition of D9 correct for any bias or offset, and E12=$a_d.(\lambda)$.

Spectral diffuse attenuation coefficient is calculated in column G according to equation 3. The spreadsheet formula is

(1/$F$3)*SQRT(F12^2+($F$3*$F$8-$F$9)*F12*(($E$3*$E$8+$E$9)*550/A12))

where (1/$F$3)=($1/\mu_0$), SQRT is the square root function, F12^2=a_t^2, ($F$3*$F$8-$F$9) calculates $G(\mu_0)$ according to equation 4, F12=a_t, and (($E$3*$E$8+$E$9)*550/A12) computes scattering coefficient, b, according to equation 6, with turbidity in cell E3=b(550), which is corrected for any linear bias or offset by the slope and intercepts in E8 and E9, respectively.

The penetration of spectral irradiance is calculated according to equation 10 in columns H and I. The spreadsheet formula in column I calculates the spectral irradiance remaining at the reference depth, z_r=$G$3, according to $H12*EXP(-$G$3*$G12). Column H is the spectrum of incident sunlight, $E_0^-(\lambda)$, taken from Weast (1977, *Handbook of chemistry and physics* 58th ed., Table F-200) and converted to units of μEinst. m^{-2} s^{-1} nm^{-1} (values at odd multiples of 5 nm above 610 nm were estimated by linear interpolation). $G$3 is the reference depth and $G12 is the previously calculated spectral diffuse attenuation, $K_d(\lambda)$.

Total PAR at the surface, PAR_0, and at the reference depth, PAR_z, are calculated by numerical integration of the appropriate spectra in cells H10 and I10, respectively. Integration is by the spreadsheet formula 2.5*(H$12+H$72)+5*SUM(H13:H71), which implements the trapezoidal rule given by

$$PAR_0 = \int_{400}^{700} E_0^-(\lambda)d\lambda \approx \frac{\Delta\lambda}{2}[E_0^-(400) + E_0^-(700)] + \Delta\lambda \sum_{i=405,410}^{695} E_0^-(i)$$

PAR_z is calculated by an analogous summation in cell I10.

The final outputs are then calculated in cells D6, E6, and F6. K_d(PAR) is calculated in cell D6 according to equation 11. The spreadsheet formula is -LN($I$9/$H$9)/$G$3, where I9 and H9 are PAR_z and PAR_0, respectively, and G3 is the reference depth, z_r.. Z_{20}(PAR) is calculated in cell E6 according to equation 2. The spreadsheet formula is -LN(0.2)/$D$6, where D6 is K_d(PAR) just described. The percentage of surface PAR remaining at the reference depth is simply $100*PAR_z/PAR_0$, which is given by the spreadsheet formula 100*$I$9/$H$9.

Table A1. Values of the cosine of the solar zenith angle, corrected for refraction at the air-water interface, and averaged over the time interval 10:00 to 14:00 standard time, as a function of day of year. Calculations are for 27.47 °N lat., 80.32 °W lon., which is the approximate location of Marker 184.

Day	Jan	Feb	Mar	Apr	May	Jun	Jul	Aug	Sep	Oct	Nov	Dec
1	0.800	0.831	0.882	0.936	0.967	0.977	0.977	0.969	0.943	0.896	0.839	0.802
2	0.800	0.833	0.884	0.938	0.967	0.977	0.977	0.968	0.942	0.894	0.837	0.801
3	0.800	0.834	0.886	0.939	0.968	0.977	0.977	0.968	0.941	0.892	0.836	0.801
4	0.800	0.836	0.888	0.940	0.969	0.977	0.977	0.967	0.939	0.890	0.834	0.800
5	0.801	0.838	0.890	0.942	0.969	0.977	0.977	0.967	0.938	0.888	0.832	0.800
6	0.801	0.839	0.892	0.943	0.970	0.978	0.977	0.966	0.937	0.887	0.831	0.799
7	0.802	0.841	0.894	0.944	0.970	0.978	0.976	0.966	0.935	0.885	0.829	0.799
8	0.803	0.843	0.895	0.945	0.971	0.978	0.976	0.965	0.934	0.883	0.828	0.798
9	0.803	0.844	0.897	0.947	0.971	0.978	0.976	0.964	0.932	0.881	0.826	0.798
10	0.804	0.846	0.899	0.948	0.971	0.978	0.976	0.964	0.931	0.879	0.825	0.798
11	0.805	0.848	0.901	0.949	0.972	0.978	0.976	0.963	0.930	0.877	0.823	0.797
12	0.806	0.850	0.903	0.950	0.972	0.978	0.976	0.962	0.928	0.875	0.822	0.797
13	0.807	0.852	0.905	0.951	0.973	0.978	0.975	0.962	0.927	0.873	0.821	0.797
14	0.808	0.853	0.907	0.952	0.973	0.978	0.975	0.961	0.925	0.871	0.819	0.797
15	0.809	0.855	0.908	0.953	0.973	0.978	0.975	0.960	0.923	0.870	0.818	0.797
16	0.810	0.857	0.910	0.954	0.974	0.978	0.975	0.959	0.922	0.868	0.817	0.797
17	0.811	0.859	0.912	0.955	0.974	0.978	0.974	0.958	0.920	0.866	0.815	0.797
18	0.812	0.861	0.914	0.956	0.974	0.978	0.974	0.958	0.919	0.864	0.814	0.796
19	0.813	0.863	0.915	0.957	0.975	0.978	0.974	0.957	0.917	0.862	0.813	0.797
20	0.814	0.865	0.917	0.958	0.975	0.978	0.974	0.956	0.915	0.860	0.812	0.797
21	0.816	0.867	0.919	0.959	0.975	0.978	0.973	0.955	0.914	0.858	0.811	0.797
22	0.817	0.869	0.921	0.960	0.975	0.978	0.973	0.954	0.912	0.856	0.810	0.797
23	0.818	0.870	0.922	0.961	0.976	0.978	0.973	0.953	0.910	0.855	0.809	0.797
24	0.819	0.872	0.924	0.962	0.976	0.978	0.972	0.952	0.908	0.853	0.808	0.798
25	0.821	0.874	0.925	0.963	0.976	0.978	0.972	0.951	0.907	0.851	0.807	0.798
26	0.822	0.876	0.927	0.963	0.976	0.978	0.972	0.950	0.905	0.849	0.806	0.798
27	0.824	0.878	0.929	0.964	0.976	0.977	0.971	0.949	0.903	0.847	0.805	0.799
28	0.825	0.880	0.930	0.965	0.976	0.977	0.971	0.948	0.901	0.846	0.804	0.799
29	0.826	////////	0.932	0.965	0.977	0.977	0.970	0.947	0.900	0.844	0.803	0.800
30	0.828	////////	0.933	0.966	0.977	0.977	0.970	0.945	0.898	0.842	0.803	0.800
31	0.830	////////	0.935	////////	0.977	////////	0.969	0.944	////////	0.841	////////	0.801

Summary of Diffuse Attenuation Coefficients for Downwelling Spectral Irradiation and Photosynthetically Active Radiation (PAR)

Jdate	Sta	Depth (m)	Time EST	Waveband (nm) 410	420	430	450	470	500	550	600	650	670	680	690	720	vis	k_d(par)
										(m^{-1})								
92342	C25S	0.5	12.14	7.587	6.511	5.548	3.885	3.508	2.187	1.487	1.116	1.128	1.106	1.094	1.141	1.703	1.614	2.148
92342	C25I	2.2	12.14	2.866	2.826	2.384	1.909	1.657	1.297	1.000	0.986	1.066	1.212	1.220	1.213	1.691	1.082	1.010
92342	172	3.5	10.28	2.645	2.382	2.102	1.583	1.366	1.043	0.751	0.752	0.861	0.998	0.993	1.009	1.535	0.865	0.910
92342	184	1.5	13.17	2.400	2.105	1.906	1.466	1.209	1.009	0.747	0.817	0.934	1.101	1.083	1.097	1.645	0.938	0.844
92342	198	1.6	15.09	2.736	2.414	2.030	1.429	1.329	1.020	0.783	0.850	0.919	1.021	1.135	1.066	1.719	0.934	0.956
92343	C25S	0.5	10.50	5.890	5.408	4.790	3.235	2.844	1.445	1.232	0.793	1.091	0.781	0.923	1.074	1.484	1.166	1.609
92343	C25I	2.5	10.50	2.851	2.315	2.148	1.707	1.453	1.082	0.858	0.867	0.991	1.074	1.118	1.124	1.610	0.975	1.064
92343	184	2.0	9.51	0.782	0.789	0.756	0.613	0.536	0.445	0.361	0.571	0.716	0.847	0.828	0.921	1.501	0.607	0.545
92343	184#2	1.8	13.42	2.052	1.734	1.607	1.330	1.167	0.964	0.745	0.824	0.954	1.111	1.171	1.108	1.677	0.932	1.052
92343	184E	0.5	13.55															1.587
92343	184ED†	0.5	13.55															1.426
92343	198	2.0	11.59	2.329	2.009	1.742	1.340	1.106	0.846	0.631	0.650	0.791	0.926	0.937	0.968	1.556	0.802	0.926
92344	C25S	0.5	12.21	6.506	5.469	4.668	3.355	2.727	2.002	1.318	1.070	1.006	1.115	1.104	1.113	1.606	1.319	1.267
92344	C25I	2.0	12.21	4.471	3.792	2.406	1.813	1.531	1.204	0.871	0.852	0.920	1.077	1.086	1.070	1.517	0.977	0.976
92344	184	1.8	11.30	1.332	1.194	1.072	0.883	0.759	0.636	0.538	0.662	0.762	0.898	0.913	0.906	1.462	0.718	0.597
92344	186	7.5	15.22	1.354	1.295	1.198	0.994	0.900	0.757	0.659	0.781	0.873	1.011	1.058	1.058	1.668	0.779	0.863
92344	198	1.7	13.46	2.307	1.982	1.771	1.282	1.187	0.941	0.664	0.782	0.871	0.973	1.005	1.032	1.571	0.876	0.928
92344	198E	1.0	N/R*															1.500
92344	198ED†	1.0	N/R															1.476
92345	C25S	0.5	13.42	5.823	5.058	4.346	3.473	3.028	2.291	1.684	1.688	1.563	1.729	1.703	1.823	2.297	1.820	1.754
92345	C25I	1.8	13.42	2.558	2.355	2.054	1.629	1.500	1.210	0.940	1.058	1.103	1.243	1.260	1.293	1.801	1.139	1.275
92345	184	1.7	13.04	1.754	1.762	1.541	1.243	0.954	0.862	0.711	0.826	0.937	1.048	1.089	1.168	1.814	0.921	0.964
92345	186	4.3	9.56	0.700	0.570	0.589	0.482	0.415	0.368	0.332	0.466	0.600	0.743	0.760	0.739	1.216	0.464	0.815

*N/R— Not Recorded †— Duplicate Profile

Summary of Diffuse Attenuation Coefficients for Downwelling Spectral Irradiation #2/3.

Jdate	Sta	Depth (m)	Time EST	Waveband (nm) 410	420	430	450	470	500	550	600	650	670	680	690	720	vis	k_d(par)
										(m^{-1})								
93060	C25S	0.5	1147	*	*	8.82	6.15	4.93	3.18	2.10	1.46	1.23	0.86	0.96	1.21	1.33	1.62	2.17
93060	C25I	2.8	1147	*	*	8.82	5.94	4.43	2.26	1.37	1.18	1.14	1.25	1.25	1.23	1.69	1.27	1.22
93060	184S	0.8	1046	*	*	3.84	2.99	2.54	1.70	1.10	0.97	0.98	1.08	1.01	0.94	1.21	1.03	2.00
93060	184I	2.1	1046		*	3.84	2.86	2.17	1.66	1.15	1.04	1.05	1.14	1.16	1.18	1.59	1.12	1.24
93060	186	8.2	1312	4.37	2.54	2.23	1.87	1.61	1.35	1.19	1.20	1.23	1.26	1.25	1.25	1.18	1.23	1.06
93060	198	2.0	1423	*	1.56	1.36	1.02	0.83	0.63	0.46	0.54	0.64	0.74	0.73	0.77	1.30	0.58	0.68
93061	C25S	0.5	1331	11.58	11.13	9.80	6.31	5.54	4.13	2.82	2.01	1.50	1.55	1.43	1.42	2.02	2.33	2.21
93061	C25I	2.8	1331	11.58	11.13	9.80	5.11	2.93	1.60	1.13	1.03	1.03	1.15	1.10	1.15	1.62	1.13	1.28
93061	184S	0.5	1237	7.85	6.46	5.43	3.93	3.25	2.19	1.47	1.22	1.06	1.05	0.96	1.16	1.73	1.39	1.54
93061	184I	2.2	1237	7.85	5.60	4.75	2.53	1.88	1.38	1.02	0.94	0.98	1.09	1.08	1.10	1.62	1.06	1.23
93061	186	7.1	1141	2.24	1.95	1.75	1.42	1.23	1.01	0.78	0.83	0.94	1.06	1.08	1.09	1.28	0.90	0.88
93061	198	1.7	1002	2.07	1.93	1.67	1.34	1.07	0.84	0.67	0.72	0.81	0.91	0.94	0.96	1.53	0.82	0.69
93062	C25S	0.5	1259	11.52	9.33	6.91	4.42	3.37	2.02	0.76	0.19	-0.07	-0.10	-0.15	-0.15	0.35	0.50	1.60
93062	C25I	2.6	1259	11.52	9.33	6.91	4.31	3.08	1.87	1.37	1.27	1.28	1.38	1.38	1.37	1.86	1.39	1.29
93062	184S	0.5	1151	2.59	2.28	1.97	1.31	1.38	1.04	0.74	0.96	0.98	0.99	1.04	1.16	1.55	1.01	1.30
93062	184I	2.2	1151	2.11	1.93	1.74	1.28	1.18	0.95	0.73	0.81	0.91	1.01	1.04	1.06	1.53	0.89	1.20
93062	186	7.5	1102	2.31	2.11	1.82	1.46	1.31	1.09	0.90	0.95	1.05	1.10	1.10	1.11	1.02	0.99	1.01
93062	198	1.5	1005	2.29	1.94	1.71	1.33	1.10	0.90	0.71	0.74	0.85	0.94	0.95	0.97	1.56	0.83	0.96
93063	C25S	0.5	1132	12.26	14.35	11.12	7.84	6.30	4.49	2.76	1.82	1.60	1.57	1.01	1.13	1.36	2.00	2.47
93063	C25I	2.7	1132	12.26	14.35	11.12	7.47	6.16	3.47	1.53	1.33	1.33	1.46	1.41	1.39	1.63	1.46	1.23
93063	184S	0.5	1226	9.34	8.43	7.30	5.58	4.52	3.40	2.27	2.00	1.64	1.43	1.51	1.36	1.98	2.24	2.41
93063	184I	2.0	1226	9.34	8.43	7.30	5.14	3.35	2.35	1.68	1.50	1.39	1.51	1.48	1.46	2.06	1.61	1.58
93063	198	2.0	1020	2.98	2.57	2.25	1.78	1.54	1.23	0.97	0.99	1.08	1.20	1.20	1.24	1.77	1.11	1.17

* — Photodetector in these channels jarred loose during transport to Ft. Pierce.

Summary of Diffuse Attenuation Coefficients #3/3

Jdate	Sta	Depth (m)	Time EST	Waveband (nm) 410	420	430	450	470	500	550	600	650	670	680	690	720	vis	k_d(par)
				(m^{-1})														
93144	198#1	2	10.14	3.618	3.647	3.17	2.62	2.315	1.945	1.596	1.516	1.547	1.655	1.639	1.637	2.141	*	*
93144	198#2	2	10.48	3.85	3.437	3.108	2.426	2.276	1.918	1.553	1.448	1.476	1.627	1.647	1.526	2.091	1.638	*
93144	198#3	2	11.55	4.005	3.575	3.259	2.612	2.317	1.989	1.581	1.507	1.327	1.671	1.668	1.577	2.115	1.671	*
93144	198#4	2	12.19	3.938	3.537	3.239	2.624	2.247	1.884	1.563	1.439	1.271	1.617	1.643	1.458	2.055	1.589	*
93144	198#5	2	12.43	3.967	3.572	3.201	2.605	2.311	1.976	1.608	1.58	1.582	1.75	1.747	1.731	2.263	1.714	*
93145	C25S#1	0.5	9.19	6.043	5.241	4.467	3.03	2.376	1.592	0.741	0.306	0.335	0.483	0.541	0.411	0.717	0.542	0.926
93145	C25I#1	2.8	9.19	5.343	4.764	3.835	3.043	2.529	2.042	1.497	1.371	1.497	1.936	1.907	1.707	1.911	1.536	1.517
93145	C25I#2	2.9	9.48	5.034	4.746	4.237	3.039	2.414	1.843	1.298	1.224	1.335	1.685	1.66	1.514	1.809	1.354	1.396
93145	C25S#2	0.5	9.48	6.87	6.018	5.191	3.911	3.182	2.571	1.674	1.236	1.365	1.723	1.959	1.639	1.895	1.497	1.842
93145	C25I#3	2.8	10.2	4.81	4.361	4.022	3.337	2.736	1.992	1.422	1.29	1.397	1.799	1.801	1.595	1.781	1.457	1.499
93145	C25S#3	0.5	10.2	5.167	4.598	4.091	3.129	2.574	1.921	1.278	1.021	1.162	1.062	1.452	1.295	1.647	1.322	1.511
93145	184#1	2.2	11.29	1.644	1.625	1.509	1.306	1.139	1.016	0.863	0.959	1.045	1.14	1.191	1.204	1.615	1.006	1.021
93145	184#2	2.2	11.55	1.689	1.564	1.466	1.251	1.122	0.97	0.803	0.924	1.037	1.099	1.13	1.154	1.691	0.996	0.982
93145	184#3	2.2	12.19	1.485	1.395	1.301	1.095	0.986	0.84	0.701	0.859	0.929	0.942	1.052	1.093	1.605	0.874	0.862
93146	198	1.7	9.37	2.965	2.661	2.39	2.033	1.808	1.513	1.232	1.221	1.252	1.35	1.355	1.369	1.86	1.329	1.386
93146	INLET	2.9	10.51	1.577	1.6	1.455	1.285	1.15	1.026	0.869	0.986	1.086	1.2	1.216	1.241	1.75	1.02	1.043
93146	184	2.2	11.42	1.7	1.602	1.478	1.258	1.125	0.967	0.811	0.918	1.003	1.021	1.158	1.134	1.56	0.881	0.951
93146	C25S	0.5	12.21	5.387	4.056	3.322	3.151	2.741	2.142	0.656	1.808	1.617	1.605	1.454	2.354	2.462	1.421	1.512
93146	C25I	2.75	12.21	5.387	4.271	3.64	3.042	2.413	1.989	1.447	1.324	1.38	1.75	1.761	1.574	1.779	1.46	1.573

* — Licor meter malfunctioned.

Water quality parameters that form primary input to optical water quality model observed during three field trips. g_{440}=absorption by filtered water at 440 nm.

Jdate	Date	Stn.	Time	μ_0	Chl ($\mu g\ L^{-1}$)	Turbidity (NTU)	g_{440} (m^{-1})
92342	7-Dec-92	172	10.28	0.79	3.94	1.80	0.852
92342	7-Dec-92	172D*	10.28	0.79	4.20	1.70	0.907
92342	7-Dec-92	184	13.17	0.79	5.17	3.25	0.652
92342	7-Dec-92	198	15.09	0.71	3.75	1.50	0.764
92342	7-Dec-92	C25I	12.14	0.81	6.48	3.70	0.806
92342	7-Dec-92	C25S	12.14	0.81	3.16	1.75	4.260
92343	8-Dec-92	184	9.51	0.77	1.81	2.25	0.140
92343	8-Dec-92	184D*	9.51	0.77	1.81	2.25	0.163
92343	8-Dec-92	184#2	13.42	0.77	4.63	3.50	0.414
92343	8-Dec-92	184E	13.55	0.77	6.13	6.40	0.477
92343	8-Dec-92	198	11.59	0.81	3.40	2.00	0.688
92343	8-Dec-92	C25I	10.50	0.80	6.09	2.80	1.124
92343	8-Dec-92	C25S	10.50	0.80	5.53	1.80	4.099
92344	9-Dec-92	184	11.30	0.81	2.27	1.75	0.131
92344	9-Dec-92	186	15.22	0.69	2.27	2.25	0.090
92344	9-Dec-92	198	13.46	0.77	3.45	2.80	0.472
92344	9-Dec-92	198E	N/R†		4.54	3.80	0.638
92344	9-Dec-92	C25I	12.21	0.81	6.19	2.30	1.197
92344	9-Dec-92	C25S	12.21	0.81	6.90	1.75	3.442
92344	9-Dec-92	C25SD*	12.21	0.81	6.22	1.70	3.201
92345	10-Dec-92	184	13.04	0.79	2.65	2.10	0.387
92345	10-Dec-92	186	9.56	0.77	2.02	1.40	0.140
92345	10-Dec-92	C25I	13.42	0.77	4.84	3.75	0.834
92345	10-Dec-92	C25ID*	13.42	0.77	5.31	3.50	0.926
92345	10-Dec-92	C25S	13.42	0.77	7.85	4.70	2.890
							0.000
92342	7-Dec-92	EQBL§	10.55		0.27	0.10	0.108
92343	8-Dec-92	EQBL	11.30		-0.06	0.10	0.154
92344	9-Dec-92	EQBL	14.30		0.09	0.10	0.062
92345	10-Dec-92	EQBL	11.30		0.08	0.14	0.025
93060	3/1/93	184I	1046	0.88	6.46	2.80	1.966
93060	3/1/93	184S	1046	0.88	2.08	1.75	5.756
93060	3/1/93	C25I	1147	0.90	6.28	2.80	2.464
93060	3/1/93	C25S	1147	0.90	1.97	2.50	6.079
93060	3/1/93	186	1312	0.88	6.51	5.80	0.589
93060	3/1/93	186D*	1312	0.88	6.27	5.50	0.636
93060	3/1/93	198	1423	0.83	1.11	1.40	0.686
93061	3/2/93	198	1002	0.84	2.03	1.80	0.543
93061	3/2/93	186	1141	0.90	4.67	2.25	0.946
93061	3/2/93	186D*	1141	0.90	4.93	2.25	0.585
93061	3/2/93	184I	1237	0.90	4.64	3.00	2.238
93061	3/2/93	184S	1237	0.90	2.50	1.90	4.835
93061	3/2/93	C25I	1331	0.87	5.40	3.75	2.068
93061	3/2/93	C25S	1331	0.87	2.20	1.90	6.309
93062	3/3/93	198	1004	0.85	1.81	2.60	0.348
93062	3/3/93	186	1102	0.89	3.45	4.00	0.776

93062	3/3/93	184I	1151	0.91	4.71	4.50	0.350
93062	3/3/93	184S	1151	0.91	4.16	3.70	0.688
93062	3/3/93	C25I	1259	0.90	4.81	3.60	2.326
93062	3/3/93	C25S	1259	0.90	2.46	2.20	6.447
93062	3/3/93	C25SD*	1259	0.90	2.36	2.20	6.724
93063	3/4/93	198	1022	0.86	2.89	2.90	0.444
93063	3/4/93	C25I	1127	0.91	4.66	3.70	3.845
93063	3/4/93	C25S	1127	0.91	2.96	1.75	8.151
93063	3/4/93	184B	1226	0.91	5.52	6.20	0.857
93063	3/4/93	184I	1226	0.91	5.45	4.75	2.130
93063	3/4/93	184ID*	1226	0.91	5.06	5.00	1.969
93063	3/4/93	184S	1226	0.91	4.53	3.25	4.628
93144	5/24/93	198#1	1014	0.96	5.77	6.20	0.771
93144	5/24/93	198#2	1048	0.98	6.56	6.25	0.603
93144	5/24/93	198#3	1155	1.00	7.47	6.25	0.497
93144	5/24/93	198#3D*			7.32	5.90	0.735
93144	5/24/93	198#4	1219	0.99	6.81	5.40	0.583
93144	5/24/93	198#5	1243	0.99	7.11	5.70	0.695
93145	5/25/93	184#1	1129	0.99	3.56	4.40	0.085
93145	5/25/93	184#2	1155	1.00	3.31	4.70	0.078
93145	5/25/93	184#3	1219	0.99	3.57	4.80	0.078
93145	5/25/93	184#3D*	1219		2.76	4.75	0.138
93145	5/25/93	C25I#1	919	0.90	25.74	4.10	0.767
93145	5/25/93	C25I#2	948	0.93	19.82	3.90	0.714
93145	5/25/93	C25I#3	1020	0.96	30.77	4.20	0.714
93145	5/25/93	C25S#1	919	0.90	10.37	1.80	2.487
93145	5/25/93	C25S#2	948	0.93	19.39	2.20	2.095
93145	5/25/93	C25S#3	1020	0.96	17.48	2.20	1.865
93146	5/26/93	184	1142	1.00	3.06	4.50	0.230
93146	5/26/93	198	937	0.92	2.80	4.00	0.447
93146	5/26/93	C25I	1221	0.99	32.14	3.90	1.142
93146	5/26/93	C25ID*	1221		31.03	4.30	0.859
93146	5/26/93	C25S	1221	0.99	20.70	2.30	2.922
93146	5/26/93	INLET	1051	0.98	2.59	4.50	0.115

*— Duplicate sample for quality control. †— Not recorded. §— Equipment Blank

Ancillary water quality data considered to be important correlates of primary optical water quality data. TSS=total suspended solids; MSS=mineral suspended solids; $a_p(400)$=absorption by particulate matter at 400 nm; $a_p(720)$=absorption by particulate matter at 720 nm.

Jdate	Date	Stn.*	Time	TSS (mg L^{-1})	MSS (mg L^{-1})	pH	Color (Pt.)	$a_p(410)$ (m^{-1})	$a_p(720)$ (m^{-1})
92342	7-Dec-92	172	10.28	8.50	6.13	8.15	10	1.034	0.343
92342	7-Dec-92	172D	10.28	5.65	3.68	8.16	10	1.000	0.235
92342	7-Dec-92	184	13.17	9.28	6.78	7.98	5	1.286	0.328
92342	7-Dec-92	198	15.09	4.76	4.00	7.89	5	0.959	0.377
92342	7-Dec-92	C25I	12.14	10.95	7.98	8.09	10	1.690	0.416
92342	7-Dec-92	C25S	12.14	4.40	2.45	7.89	65	1.750	0.142
92343	8-Dec-92	184	9.51	8.65	6.93	8.18	6	0.706	0.212
92343	8-Dec-92	184D	9.51	7.10	4.90	8.19	5	0.734	0.229
92343	8-Dec-92	184#2	13.42	9.89	7.56	8.11	5	1.311	0.433
92343	8-Dec-92	184E	13.55	28.60	22.85	8.02	6	2.143	0.694
92343	8-Dec-92	198	11.59	7.43	5.66	8.06	5	1.042	0.371
92343	8-Dec-92	C25I	10.50	8.48	6.10	7.89	8	1.690	0.478
92343	8-Dec-92	C25S	10.50	4.23	2.48	7.72	50	1.826	0.356
92344	9-Dec-92	184	11.30	7.64	5.72	8.20	5	0.901	0.314
92344	9-Dec-92	186	15.22	8.16	5.91	7.94	4	0.981	0.303
92344	9-Dec-92	198	13.46	9.28	7.25	8.01	6	1.290	0.401
92344	9-Dec-92	198E		16.37	11.82	8.14	8	2.348	0.765
92344	9-Dec-92	C25I	12.21	8.38	6.05	8.01	12	1.308	0.316
92344	9-Dec-92	C25S	12.21	4.95	2.73	7.81	45	1.897	0.373
92344	9-Dec-92	C25SD	12.21	5.10	3.20	7.78	45	1.954	0.380
92345	10-Dec-92	184	13.04	6.09	4.56	8.09	6	0.987	0.297
92345	10-Dec-92	186	9.56	6.42	4.58	8.07	5	0.641	0.214
92345	10-Dec-92	C25I	13.42	14.23	11.14	7.97	15	2.120	0.676
92345	10-Dec-92	C25ID	13.42	10.58	7.90	7.94	15	1.874	0.561
92345	10-Dec-92	C25S	13.42	11.23	7.74	7.86	42	3.089	1.062
92342	7-Dec-92	EQBL	10.55	0.13	-0.65	5.80	0	-0.007	-0.022
92343	8-Dec-92	EQBL	11.30	0.25	-0.35	5.60	0	0.042	0.024
92344	9-Dec-92	EQBL	14.30	0.43	-0.13	6.35	0	-0.007	-0.008
92345	10-Dec-92	EQBL	11.30	0.35	-0.01	6.24	0	0.066	-0.005

Ancillary water quality data, continued.

Jdate	Date	Stn.	Time	TSS (mg L^{-1})	MSS (mg L^{-1})	pH	Color (Pt.)	$a_p(400)$ (m^{-1})
93060	1-Mar-93	184I	1046	15.65	12.10	7.99	32	1.400
93060	1-Mar-93	184S	1046	7.12	5.00	7.67	90	1.496
93060	1-Mar-93	C25I	1147	9.66	6.74	7.76	30	1.596
93060	1-Mar-93	C25S	1147	4.53	3.09	7.47	80	1.510
93060	1-Mar-93	186	1312	37.43	31.05	7.85	8	1.559
93060	1-Mar-93	186D	1312	45.80	37.90	7.86	8	1.706
93060	1-Mar-93	198	1423	8.11	6.47	7.92	8	0.436
93061	2-Mar-93	198	1002	10.75	8.23	7.97	10	1.069
93061	2-Mar-93	186	1141	10.66	7.92	7.93	15	0.948
93061	2-Mar-93	186D	1141	10.60	7.89	7.94	15	0.951
93061	2-Mar-93	184I	1237	10.91	8.03	7.87	28	1.429
93061	2-Mar-93	184S	1237	10.12	7.83	7.60	65	1.595
93061	2-Mar-93	C25I	1331	12.50	8.93	7.85	25	1.620
93061	2-Mar-93	C25S	1331	4.30	2.47	7.47	80	1.448
93062	3-Mar-93	198	1004	10.49	8.55	8.06	5	1.029
93062	3-Mar-93	186	1102	16.09	12.92	8.02	13	1.194
93062	3-Mar-93	184I	1151	13.65	10.33	8.01	7	1.329
93062	3-Mar-93	184S	1151	11.00	8.09	7.97	17	1.194
93062	3-Mar-93	C25I	1259	11.82	8.65	7.86	35	1.342
93062	3-Mar-93	C25S	1259	3.79	2.29	7.55	80	1.448
93062	3-Mar-93	C25SD	1259	3.69	2.46	7.57	78	1.475
93063	4-Mar-93	198	1022	10.23	8.06	8.09	10	1.408
93063	4-Mar-93	C25I	1127	10.47	7.24	7.81	47	1.695
93063	4-Mar-93	C25S	1127	4.33	2.50	7.63	94	1.389
93063	4-Mar-93	184B	1226	21.96	17.00	8.10	12	2.068
93063	4-Mar-93	184I	1226	16.27	11.77	8.01	32	1.935
93063	4-Mar-93	184ID	1226	16.18	11.88	8.04	32	1.757
93063	4-Mar-93	184S	1226	10.50	7.30	7.84	58	1.509

Ancillary water quality data continued.

Jdate	Date	Stn.	Time	TSS (mg L^{-1})	MSS (mg L^{-1})	pH	Color (Pt.)	$a_p(400)$ (m^{-1})
93144	5/24/93	198#1	1014	25.70	19.95	7.90	10	2.720
93144	5/24/93	198#2	1048	24.71	19.36	7.92	10	2.514
93144	5/24/93	198#3	1155	26.24	21.06	7.95	11	2.573
93144	5/24/93	198#3D		24.24	19.06	7.96	11	2.482
93144	5/24/93	198#4	1219	21.36	16.59	7.94	11	2.499
93144	5/24/93	198#5	1243	19.71	15.59	7.92	12	2.380
93145	5/25/93	184#1	1129	16.50	11.88	8.16	6	1.371
93145	5/25/93	184#2	1155	21.39	16.31	8.18	7	1.357
93145	5/25/93	184#3	1219	18.77	14.20	8.19	5	1.207
93145	5/25/93	184#3D	1219	19.40	14.07	8.20	5	1.130
93145	5/25/93	C25I#1	919	16.34	12.00	8.11	13	1.837
93145	5/25/93	C25I#2	948	17.84	12.34	8.06	14	1.706
93145	5/25/93	C25I#3	1020	17.83	11.56	8.14	14	1.751
93145	5/25/93	C25S#1	919	11.34	8.50	8.02	42	1.654
93145	5/25/93	C25S#2	948	7.12	4.08	8.00	37	1.575
93145	5/25/93	C25S#3	1020	8.33	4.75	8.09	34	1.438
93146	5/26/93	184	1142	17.13	12.44	8.12	5	1.365
93146	5/26/93	198	937	38.06	30.95	8.13	10	2.093
93146	5/26/93	C25I	1221	13.11	8.34	8.14	18	2.015
93146	5/26/93	C25ID	1221	17.34	10.88	8.12	17	2.111
93146	5/26/93	C25S	1221	10.35	5.20	8.05	43	2.069
93146	5/26/93	INLET	1051	20.04	15.00	8.08	3	1.304